University of Reading
School of Mathematics, Meteorology and Physics

'Every snowflake is different'

Investigating the effect of the variability in snowflake shape on aggregation

by
Victoria J. Heighton

August 18, 2008

This dissertation is submitted to the Department of Mathematics and Meteorology in partial fulfilment of the requirements for the degree of Master of Science

Abstract

Ice crystal aggregation is of great importance in understanding and predicting precipitation in the UK. It is also highly influential in climate prediction through its influence on cloud properties. It is therefore important to keep striving for a better understanding of the mechanism and better methods for its reproduction in models.

Many previous models and studies have assumed relationships on ice particle parameters, including fitted area- and mass-diameter relationships. However, these relationships eliminate the variability of these parameters and mean that no account is taken of the effect of the individual snowflake's shape.

This dissertation reviews previous research into ice crystal aggregation modelling and observations. It also investigates the problem using a new modified Monte Carlo model which employs fall speed equations that are based on the individual particle's shape, as every snowflake has its own geometry, and consequently fall speed. Investigation into the fall speeds showed that the dispersion of the fall speeds between large snowflakes of different sizes does not reduce to negligible amounts as previously expected in other studies. This was also reflected in the results on the relationship between the parameters N_0 and λ characterising the slope and intercept of the approximately exponential snowflake size distribution. It was found that λ steadily decreased to values of λ below 10cm^{-1} contradicting other studies that have suggested that the relationship would alter dramatically at this point, possibly as a result of aggregation slowing to a negligible rate through a reduction in the dispersion of fall velocities for large snowflakes. Comparison with radar data showed that the new modified Monte Carlo model also provided an reasonable reproduction of the obervered approximately exponential relationship between reflectivity and time.

The results were also compared to results produced by simplified models, employing fall speed calculations not dependent on individual particle's shapes. Comparison plots of the radar reflectivity against time for the models showed that the simplified models exhibited a much slower aggregation rate. The implications for using data from radar to observe properties of ice crystals in clouds using Doppler spectra were also investigated.

Declaration

I confirm that this is my own work, and the use of all material from other sources has been properly and fully acknowledged.

Victoria J. Heighton

Acknowledgements

I would like to thank my supervisors Chris Westbrook for his patience, enthusiasm and support and Robin Hogan for his valuable contributions. I would like to acknowledge the financial support of the NERC for the Masters programme 2007-08. I would also like to thank my family for their unending support and love and my friends for always helping me keep my mind on happier, shinier things.

An Outdoor Hum for Snowy Weather

"The more it snows
(Tiddly Pom)
The more it goes
(Tiddly Pom)
The more it goes
(Tiddly Pom)
On snowing.

And nobody knows
(Tiddly Pom)
How cold my toes
(Tiddly Pom)
How cold my toes
(Tiddly Pom)
Are growing."

A.A.Milne

Contents

List of Figures

Chapter 1

Ice Crystals, Snow Flakes and Aggregation

This first chapter aims to provide the background knowledge on which this project is based or direct the reader to where it can be obtained. This chapter will provide an overview to the relevance of aggregation to the weather and climate, though ice nucleation and growth processes in clouds.

1.1 Why is it important?

Modelling and understanding what happens to ice crystals in clouds is integral to furthering our understanding and ability to model the weather and the climate.

Correctly predicting precipitation is of paramount importance for many things from agriculture to flood warnings in towns and shipping forecasts and this in turn depends on the understanding of the processes which create it. In the United Kingdom the majority of the rain that falls is attributable to melting ice particles. This is due to the Bergeron Findeisen Process, see section 1.2, which occurs where a small number of ice crystals grow large at the expense of liquid water droplets. The large ice crystals then fall and become an efficient source of precipitation and furthermore can seed liquid clouds.

It is also important for improving modelling and understanding the climate. At any point in time around 1/4 of the surface of the earth is covered by cirrus clouds [23] which are composed of ice crystals and aggregate snowflakes. The climatic effect of cirrus clouds is in general a warming. As seen in the Intergovernmental Panel on Climate Change (IPCC)'s fourth assessment report [27, p. 38], clouds are one of the biggest uncertainties in predictions of climate change. Deep stratiform ice clouds associated with weather

fronts could have a cooling effect due to their optical thickness, reflecting solar radiation back into space. Therefore it is important to understand the growth of ice crystals in these clouds in order to predict their radiative properties better. Sensitivity studies with the ECMWF global forecast model have shown that changes in the parameterised ice particle fall speeds, within a realistic range, can have a large impact changing the global mean net flux by as much as $10\mathrm{Wm}^{-2}$, as seen in [28, fig. 1]. It is also important to improve ice particle aggregation modelling as it is an important growth mechanism, and increases the fall speeds because of this.

1.2 Nucleation

Ice clouds form as moist air rises in the atmosphere. The associated fall in pressure causes the air to expand adiabatically and to cool. As the air becomes supersaturated water droplets are formed on cloud condensation nuclei, of which the atmosphere has an ample supply. If the droplet is cooled to a sufficiently low temperature then it will freeze, forming an ice crystal by one of two mechanisms: homogeneous nucleation and heterogeneous nucleation.

In general homogeneous nucleation is reserved for clouds where the temperature is $-40°\mathrm{C}$ or lower and as such is mainly the reserve of high clouds like cirrus. For the droplet to freeze through homogeneous nucleation, some of the water molecules within the droplet must form into an ice-like lattice structure. If this happens by chance then the droplet then freezes around these lattice structures. Experimental observations have shown that this occurs at $\approx -40°\mathrm{C}$ for the size of droplets that are relevant to the atmosphere [29].

Heterogeneous nucleation however can occur when the temperature is above $-40°\mathrm{C}$ and requires the presence of aerosols to serve as a nucleus around which freezing can occur. Only certain substances are effective as an ice nuclei and this includes clay particles and desert dust; artificial nuclei include silver iodide and dry ice, the latter being the basis of cloud seeding. The effectiveness of ice nuclei increases as the temperature reduces. Due to the relative sparseness of ice nuclei, ice crystals formed through heterogeneous nucleation and supercooled water droplets co-exist in clouds. However this situation can result in the Bergeron Findeisen Process which occurs because the saturation vapour pressure over ice is always greater than that over liquid water. This causes the ice crystal to grow in the water saturated conditions, which depletes the available water vapour, making the air subsaturated with respect to the water droplets, which causes them to evaporate. Thus the ice crystals grow large at the expense of the water

droplets.

1.3 Growth mechanisms

Initially the ice crystals grow by the deposition of water vapour onto the surface of the ice crystal. This dominates the growth of the particle near the top of the cloud where the ice crystals are small and have small fall speeds. As the crystals get larger and they begin to fall through the cloud their growth is often dominated by aggregation. Aggregation occurs when ice crystals collide and may form a bond attaching them to each other therefore forming an 'aggregate'. The mechanics involved in the bond are still a matter of research. Sticking mechanisms that have been suggested include: mechanical interlocking, sintering, vapour deposition, electrical forces also known as attraction and a 'sticky' liquid-like layer on the surface of the ice crystal. In older observational studies it was suggested that ice crystal aggregation became inefficient in temperatures $< -20°C$. However, as improvements have been made in the imaging probes used to obtain measurements from aircraft, aggregates have been found at temperatures of $-40°C$ and below [26]. In [30] Mason suggests that the bonding between ice crystals is in part due to interlocking and to sintering, where the surface attempts to minimise surface energy in the places the crystals touch forming a bridge between the crystals. Mason further suggests that if the air surrounding the two particles is supersaturated over ice then vapour deposition on the surface of the crystals 'may act as cement' [30, p. 249]. In [30] the assumption, that aggregation is not efficient at temperatures below $-20°C$, is further dispelled with references to a study by Hosler et al [31] where adhesion of ice spheres are measured at temperatures down to $-80°C$. Aggregate formation is not the only possible outcome of two ice crystals colliding, they may simply change paths or break on impact.

There is one other mechanism by which ice crystals can grow and that is riming. This is when the falling ice crystal gains size as supercooled water droplets in its path deposit upon it. This dissertation will concentrate only on the growth of ice crystals in glaciated clouds by aggregation, where bonds between crystals are formed on impact, figure 1.2 shows some examples of aggregates.

1.4 Ice crystal types

There are many different ice crystal types, described by their geometrical appearance, degree of riming and degree of aggregation.

Figure 1.1: Some examples of ice crystal types, from left to right, hexagonal plate, bullet rossette and dendrite, taken from [25] and [26]

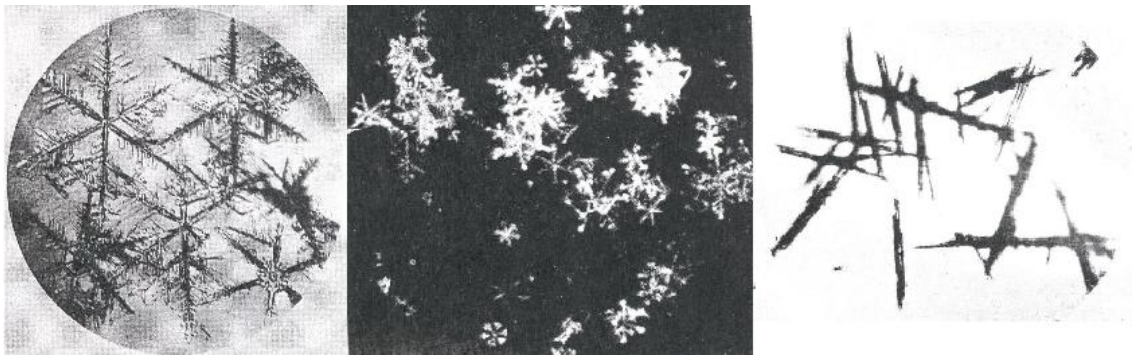

Figure 1.2: Some examples of aggregates, from left to tight, dendrite aggregate, snowflakes composed of dendrite aggregates, needle-like crystal aggregate, taken from [30] and [32].

Figure 1.1 shows some example of different crystal types and figure 1.2 has images of examples of aggregates of different crystal types.

There are several different categorisation systems which generally focus in particular on one aspect. Different types are usually identified in studies using images, and data for different types is usually treated separately.

Different types of ice crystal are known to grow at different temperatures and humidities as shown in figure 1.3. Planar growth, of plates and dendrites, is seen in temperatures between approximately $-10°C$ and $-20°C$. Columns are observed to grow in approximate temperature regimes of $< -20°C$ and $-3°C$ to $-10°C$. Plates are also observed growing for temperatures above $-3°C$. The more complex ice crystals shapes of the branched and dendritic types grow at higher supersaturations. Bullet rossettes and side planes form at the coldest temperatures below $-20°C$.

As a crystal grows larger it begins to fall, which sometimes will take the crystal into a different temperature regime. This can cause a mixture of crystal types, like plates

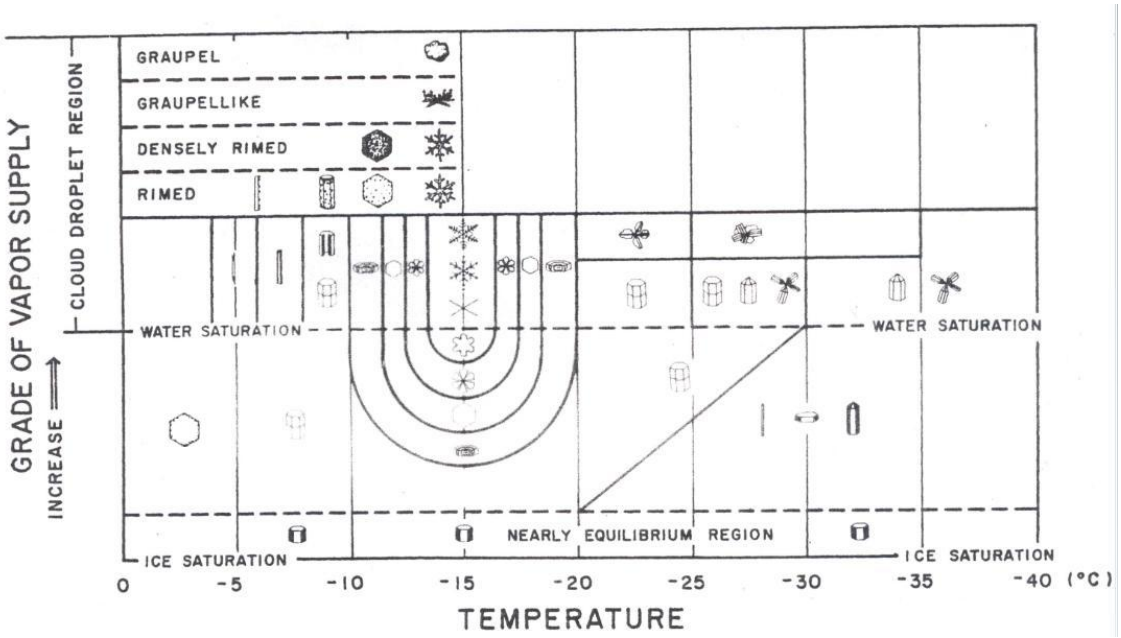

Figure 1.3: Diagram depicting the conditions, in temperature and humidity, in which various ice crystal types form, taken from [32]

growing on the end of column crystals as seen figure 1.4.

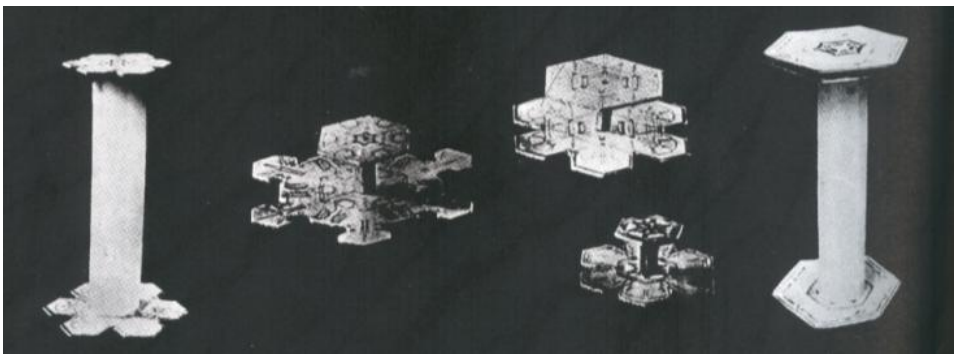

Figure 1.4: Examples of plate ice crystals growing by vapour deposition on the end of column ice crystals, taken from [33]

Chapter 2

Previous observations and modelling of snowflake fall speeds and aggregation

In this chapter I hope to familiarise the reader with previous work on the subject of ice crystal aggregation both in observation and modelling. Previous models and their results are clearly very important in order to build a basis on which to build future improved models, however, observational studies are also very important for models and modelling. They serve as a benchmark against which a model's accuracy can be measured. As modelling techniques and models improve and have greater refinement there is a demand for increasingly detailed observational measurements and less fallible techniques and instrumentation.

This chapter firstly provides a review of previous work on aggregation, particularly those which relate to the fall speeds of ice particles. These are particularly important as the fall speeds control the aggregation process through collisions produced by ice particles falling at different velocities. Then observational measurements, taken from aircraft, of snowflakes in stratiform clouds are also reviewed, to give indication of the effect of aggregation on ice particle size distributions, and suggestions for what other processes may be occurring in those clouds. The final part of this chapter shall detail and discuss how other studies have attempted to model the process.

2.1 Observations and modelling of ice particle fall velocities

2.1.1 Observational studies

In their 1974 [13] Locatelli and Hobbs claimed that although experimental observations had been gathered before, the data sets available were "still scatty and inadequate for many purposes" and some "show inconsistencies" with an overall pattern not yet obvious [13, p. 2185].

Locatelli and Hobbs measured the fall speed of particles using two parallel light beams placed vertically above one another. Any decrease in the intensity of either beam is recorded as the passing of the ice particle through that beam. As the exact distance between the two beams is known the time difference between a particle passing through the first and the second beam can be used to calculate its fall speed. A thin piece of plastic, 'Handiwrap' below the beams was used to catch the particles so other observations could be made. The dimensions of the particles were then taken using microphotographs and after the particles were melted the size of the remaining water droplet (or sometimes droplets in the case of aggregates) enabled an estimate of the mass to be obtained.

Through an advance in data gathering technique, there are still potential problems. It is possible for two particles to be passing through the beams at the same time and though this can be monitored and any data from such an occurrence ignored, it makes the method very time consuming. The possibility of a very large particle crossing both beams at once is negated by separating the two beams by twice as much as the dimension of the largest particle. Although Locatelli and Hobbs highlight the problem of having too many classifications of ice particles, they use the same classification system, Magono and Lee [14], as the problem was highlighted in.

The study did produce some important general patterns within the data for different particle types. With enough data for a particular particle type, the physical properties were presumed to fit a relationship of the form $y = ax^b$ and a logarithmic conversion of the data was used to find a and b. For most of the particle types studied, Locatelli and Hobbs produced an estimated relationship for velocity-dimension, velocity-mass and mass-dimension which can be found in the table in [13, p. 2188].

In comparing their findings with those of other studies Locatelli and Hobbs look at a study by Zikmunda and Vali [15]. In this study a basic relationship of $y = a + b\log D$ is assumed rather than $y = ax^b$. By using graphical representations of these relationships

and the gathered data for particular particle types, Locatelli and Hobbs argue that their assumption is closer to reality than Zikmunda and Vali.

In [13], general features of the measurements were examined and general relationships between particles were determined using best fits. The velocity-diameter relationship is approximated, for different types of aggregates. As can be seen in figure 2.1 the

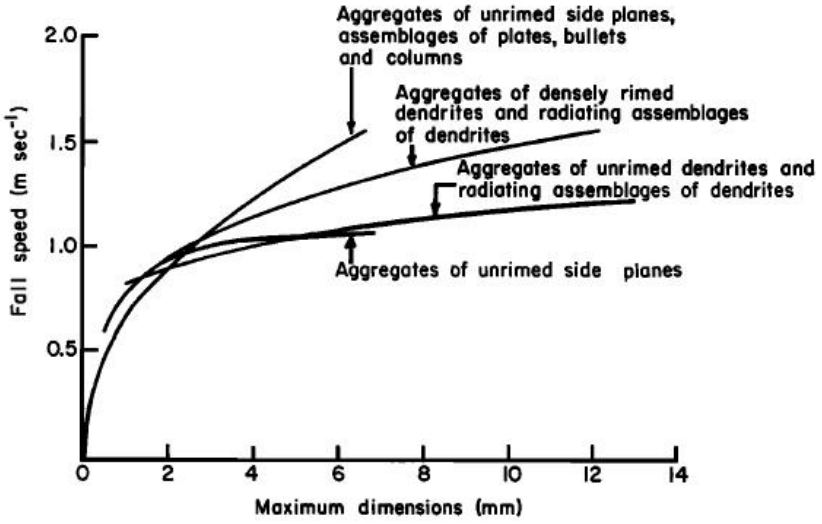

Figure 2.1: Best Fit curves for velocity-diameter relationship as shown in [13, p. 2194]

velocity-diameter relationship is of a similar form for all aggregate types, though the scale differs. It can be particularly observed that on average, given sufficient observations of large aggregates, the velocity at larger sizes of aggregates tends to flatten out.

Locatelli and Hobbs also investigated the mass-diameter relationship approximating it in a similar manner to the velocity-diameter relationship to produce general relationships, as seen in figure 2.2. The mass-diameter relationship for all types aggregates are very similar. These power law relationships for mass and diameter are important for converting measurements taken of a particle's diameter and converting it into an approximation of its mass, as is seen in many airborne observational studies, and for parameterising ice particles in NWP models, for example the Met Office's Unified model. They also gain importance in light of the fact that a power law relationship for mass and diameter is often assumed in subsequent studies of models of fall speeds and aggregation in clouds.

Barthazy and Schefold conducted a more recent investigation into fall speeds of crystals according to their type and the degree of riming [20]. Like Locatelli and Hobbs they also employed ground-based instrumentation in order to gain more accurate fall speed measurements though, as for Locatelli and Hobbs, this limits the results to snowfall

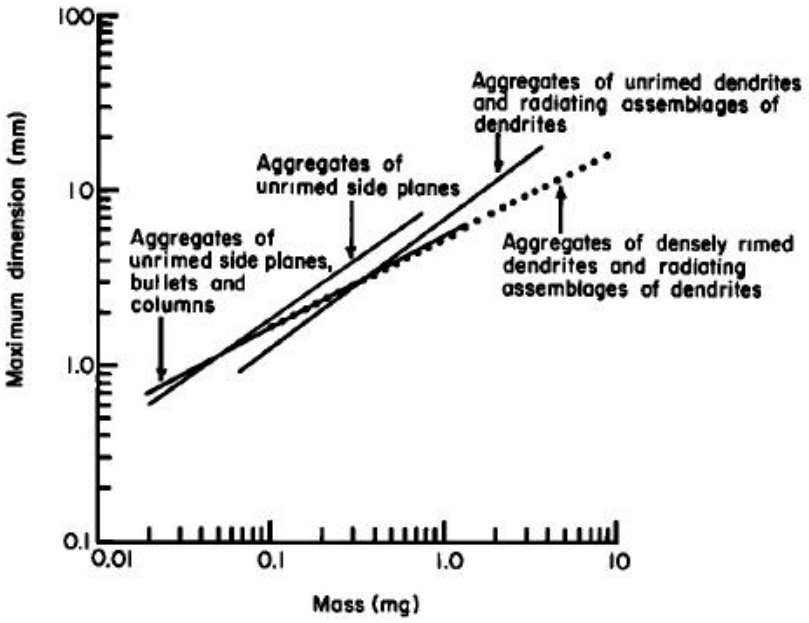

Figure 2.2: Best fit curves for the mass-diameter relationship as shown in [13, p. 2194]

that reaches the ground. The measurements are gathered using the hydrometeor velocity and shape detector, HSVD, an optical instrument that measures the velocity using two beams of light as Locatelli and Hobbs [13] had done but which also took images as the beams were broken, eliminating some of the problems Locatelli and Hobbs had faced, meaning more measurements could be made. The image is a side-view of the particle and is used to calculate the diameter of the particle, the particle's type and the degree of riming was ascertained by taking samples on microscope slides. When a crystal type and riming degree is ascertained for a particular sample all HSVD gathered data in the 30 seconds preceding or following the gathering of that sample is presumed to have the same type and riming degree. This is not of course what occurs in reality but is useful for investigative purposes.

Barthazy and Schefold used two separate equation forms to fit the data a power law and an exponential function:

$$v\left(D\right) = \alpha D^{\beta}$$

$$v\left(D\right) = a\left(1 - e^{-bD}\right)$$

where a, b, α and β are constant coefficients.

They found that both of these fits depended on the degree of riming measured only when used on the data attributed to needle and plate crystals types. For the data on needle and plate crystals there was an observable increase in the degree of riming which

corresponded to an increase in fall speed. Though the fall speeds of all crystal types and riming degrees exhibit generally similar relationships in these observations it is necessary to recall the way in which these types and degrees were attributed to them and how this may have mixed the data for each to a certain degree. For aggregates, the estimated power-law velocity-diameter relationships were similar to those of Locatelli and Hobbs and for the largest unrimed aggregates the velocity appears almost constant on average.

2.1.2 Theoretical treatment of the ice particle's fall speed

Empirical expressions, often in the form of power laws, for the fall speeds of ice particles have been estimated from observational data and used in many studies and NWP models, for example the Met Office model [17].

In his paper [5] published in 1996, Mitchell sets forward an improved method of calculation of the terminal velocity of ice particles from their size and shape and compares the results with previous studies.

The drag force on a particle in a fluid is given by:

$$F_D = \frac{1}{2}\rho_a v^2 A C_D \tag{2.1}$$

where ρ_a is the density of the air, v the velocity of the particle, A the area projected by the particle perpendicular to the flow and C_D is the drag coefficient. For large Reynolds numbers $\mathrm{Re} = DV/\nu_k$, e.g. large snowflakes, the drag coefficient is approximately constant, and Mitchell estimates that in this situation $C_D = C_0 = 0.6$. For smaller Reynolds numbers the drag coefficient is not constant but varies with the Reynolds number $C_D = C_D\,(\mathrm{Re})$.

The terminal velocity, v, can then be calculated by equating the gravitational force mg with the drag force, thus producing the formula:

$$v = \left(\frac{2mg}{\rho_a A C_D}\right)^{\frac{1}{2}} \tag{2.2}$$

Unfortunately C_D is itself a function of Re and therefore of v.

In order to avoid this dependence on v in the calculation, Mitchell utilises the Best or Davies Number, X. The Best Number can be calculated without using v:

$$X = C_D \mathrm{Re}^2 = \frac{2mg\rho_a D^2}{A\eta^2} \tag{2.3}$$

where D is the maximum dimension of the particle, η is the dynamic viscosity, Re the

Reynolds number of the particle. The Best number depends on the projected area, mass and maximum dimension of the particle.

Given knowledge of the particle shape or measurements of mass, area and the maximum dimension the best number can be calculated directly. A number of experimental and observational studies have measured Re-X relationships; Mitchell attempts to unify them into a single theory. Once *Re* has been calculated from X, the terminal velocity can be directly calculated from:

$$v = \frac{\mathrm{Re}\nu_k}{D} = \frac{\mathrm{Re}\rho_a}{D\eta} \tag{2.4}$$

where ν is the kinematic viscosity and η is the dynamic viscosity.

Boundary layer theory is applied to the problem as hypothesized for a sphere by Abraham [6]. The particle is assumed to have an attached boundary layer surrounding it of width δ as shown in Figure 2.3. The ice particle and boundary layer are treated as a solid body, and the flow around the assembly of the particle with its attached boundary layer is assumed to be inviscid.

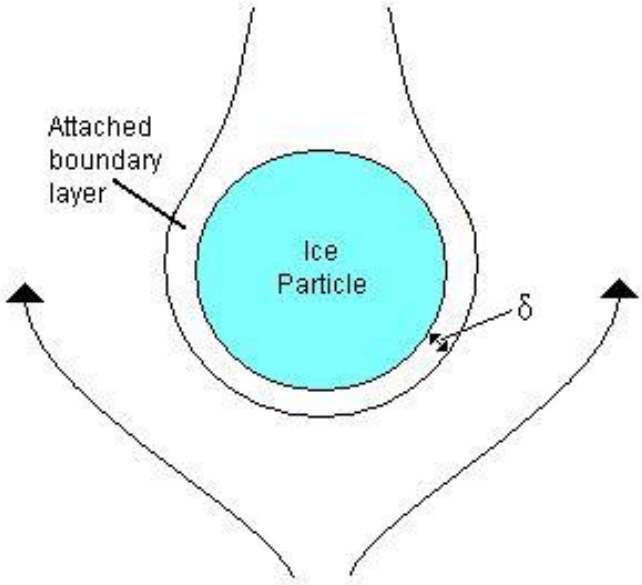

Figure 2.3: Boundary layer view of an ice particle

So we now simply require the drag on the entire assembly, Σ, of the ice particle and its surrounding boundary layer. From equation (2.1) the drag is:

$$F_D = \frac{1}{2}\rho v^2 C_0 A_\Sigma \tag{2.5}$$

where A_Σ is the projected area of the ice particle and the attached boundary layer. C_0 the drag coefficient is now constant as the flow around Σ is inviscid, corresponding to $\nu_k << 1$ and therefore the Reynolds number of the assembly is large. Mitchell assumes that A_Σ can be estimated by:

$$A_\Sigma = \pi \left[r_{eq} + \delta\right]^2 \tag{2.6}$$

where r_{eq} is the radius of the sphere equivalent in projected area to that of the ice particle. Boundary layer theory provides the equation:

$$\delta = \frac{\delta_0 r_{eq}}{\sqrt{\mathrm{Re}}} \tag{2.7}$$

where δ_0 is a constant, as in [5].

Combining equations 2.1, 2.3, 2.6 and 2.7 A general relationship between Re and X is then produced:

$$\mathrm{Re} = \frac{\delta_0^2}{4}\left[\left(1 + \frac{4X^{1/2}}{\delta_0^2 C_0^{1/2}}\right)^{1/2} - 1\right]^2 \tag{2.8}$$

This continuous analytical relationship can be used to calculate the terminal velocity, provided the mass and area-dimensional relationships are known, or can be estimated with a good degree of accuracy.

Previous observational studies [7], [8] have leaned toward the power-law relationship:

$$\mathrm{Re} = aX^b \tag{2.9}$$

and subsequent fall speed expression:

$$v = \frac{a\nu}{D}\left(\frac{2mD^2 g}{\rho_a \nu^2 A}\right)^b \tag{2.10}$$

Mitchell proposes a simple method to parameterise the Best number, using mass and area projected normal to the flow expressed in the form of a power law of the maximum dimension:

$$m = \alpha D^\beta \tag{2.11}$$

$$A = \gamma D^\sigma \tag{2.12}$$

So obtaining the expression:

$$X = \frac{2\alpha g \rho_a D^{\beta+2-\sigma}}{\gamma \eta^2} \tag{2.13}$$

Based on equation (2.8) the Re-X relationship can be approximated by:

$$\mathrm{Re} = 0.04394X^{0.970}, 0.01 < X \leq 10.0 \tag{2.14}$$

$$\mathrm{Re} = 0.06049X^{0.831}, 10 < X \leq 585 \tag{2.15}$$

$$\mathrm{Re} = 0.2072X^{0.638}, 585 < X \leq 1.56x10^5 \tag{2.16}$$

$$\mathrm{Re} = 1.0865X^{0.499}, 1.56x10^5 < X \leq 10^8 \tag{2.17}$$

Though (2.8) is a continuous function it can be approximated using this series of power

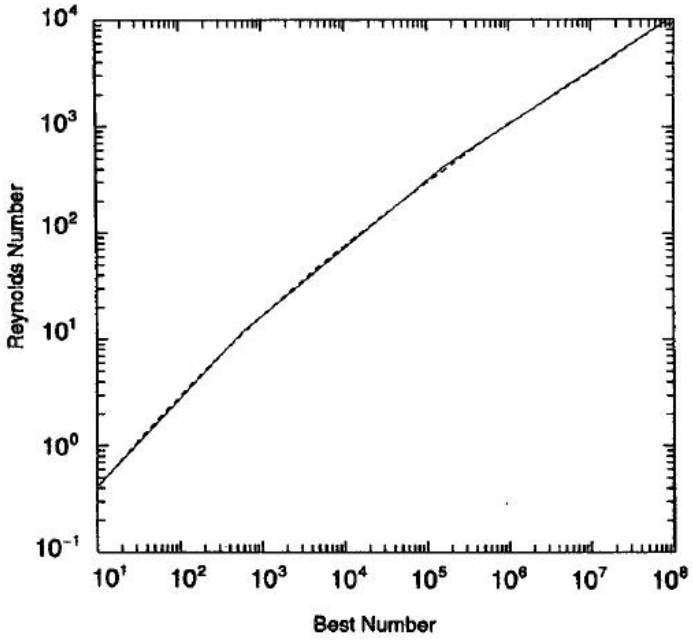

Figure 2.4: The dashed line represents equation (2.8) and its approximations (2.15), (2.16) and (2.17) are given by the straight solid lines, taken from [5, p. 1715]

laws over a limited range.

So these parameters can be input as a and b into the equation derived from (2.11), (2.12) and (2.10):

$$v = a\nu \left(\frac{2\alpha g}{\rho_a \nu^2 \gamma} \right)^b D^{b(\beta+2-\sigma)-1} \tag{2.18}$$

with α, β, γ and σ dependent on the projected area and mass of the particle. A table compiled from several sources is contained in the paper [5] containing values for the parameters dependent on the particle type and its size.

Mitchell and Heymsfield published refinements to the method in 2005 [9]. They made a minor correction to the method for turbulent flow around aggregates at very

high Reynolds numbers. This only has implications for the very largest ice particles however.

Mitchell and Heymsfield compared several different Re-X relationships from different studies: The second highest (short dashed) curve in Figure (2.5) represents

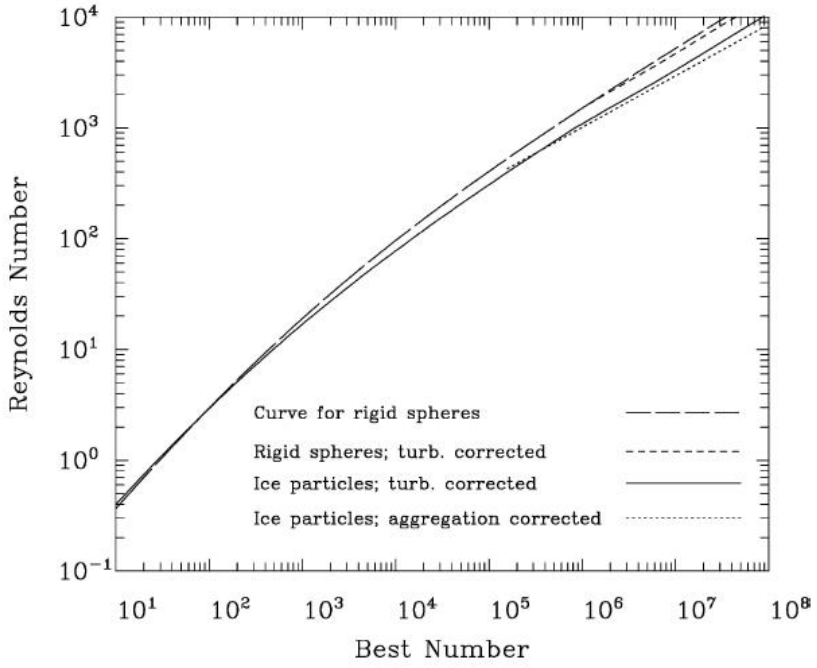

Figure 2.5: Figure taken from [5, p. 1639] illustrating the different Re-X relationships produced

Khvorostyanov and Curry's solution [10]. They expressed (2.8) in the form of a power law $\mathrm{Re} = a\,(X)\,X^{b(X)}$ using parameters equivalent to $\delta_0 = 9.06$ and $C_0 = 0.292$, which Mitchell and Heymsfield argue are more appropriate for modelling smooth rigid spheres like water drops than ice particles and aggregates. Heymsfield et al. [11] used measurements of aggregates to propose a Re-X relationship that suggested that equation (2.8) overestimates the fall speeds of the largest snowflakes by 15%. However, Mitchell and Heymsfield [9, p. 1638] suggest that caution needs to be exercised towards these measurements due to possible systematic bias in the measurement of the projected area. This Re-X relationship is illustrated in Figure 2.5 by the lowest (dotted) line though the possible bias would effect it by overestimating the area and therefore underestimating the Best number, X. The second lowest (solid) line is produced by (2.8) with $\delta_0 = 5.83$ and $C_0 = 0.6$ as used in Mitchell's 1996 paper [5]. Mitchell and Heymsfield hypothesise that deviations of the lowest (dotted) line from the second lowest (solid) line are due to alterations in δ_0 and/or C_0, since for $X > 10^6$ $C_D \approx C_0 \approx 0.6$ [12], it is likely that these

alterations are in δ_0. From (2.8) an increase in δ_0 for aggregates could account for a decreased Reynolds number with respect to the Best number as the lowest line in Figure (2.5) from [11] suggests, it would also produce an increase in the effective area of the assembly Σ in boundary layer theory and therefore a decrease in the terminal velocity.

For aggregates Mitchell and Heymsfield propose the following altered relationship for aggregates:

$$\mathrm{Re} = \frac{\delta_0^2}{4}\left[\left(1 + \frac{4X^{1/2}}{\delta_0^2 C_0^{1/2}}\right)^{1/2} - 1\right]^2 - a_0 X^{b_0} \tag{2.19}$$

where for $a_0 = 1.7 \times 10^{-3}$ and $b_0 = 0.8$. This equation provides the best fit to the available fall speed data and is the fall speed equation that will be used in modelling the aggregation of ice crystals in chapter 3. The additional second term in the equation is proposed to account for the dilation of δ_0 and subsequent increase in the effective area as they found simply adjusting constants δ_0 and C_0 was not sufficient.

The Monte Carlo model in section 2.3.3 and chapter 3 resolves the geometry of the aggregates, therefore the mass, the projected area and the maximum dimension are all known and need not be estimated by power-law relationships as it is in other studies. The Best number can be calculated using (2.3) and the Reynolds number by (2.19). Then the terminal velocity can be calculated using the relationship (2.4) rearranged to give $\upsilon_t = \mathrm{Re}\nu/D = \mathrm{Re}\rho_a/D\eta$.

2.2 Observations of aggregation in ice clouds

Lo and Passarelli Jr.'s 1982 study [16] was published as an attempt to produce observational data that could give a 4-dimensional (in space and time) picture of the properties of the ice crystals throughout their growth history. A major constraint on the solution of this problem is that all the data be gathered by just one aeroplane in just a single flight. Another question is whether the technology will be able to differentiate between the effects of different physical processes.

Another significant factor in the development of the sampling procedure is the horizontal movement of particles exhibited by all ice particles even in steady conditions. To produce a simple model of this behaviour, assuming a steady, finite source, Lo and Passarelli used the equation:

$$X = X_0 + \frac{S}{2}\frac{(Z_0 - Z)^2}{v} \tag{2.20}$$

where X is the particle's horizontal position with respect to its origin X_0, S is the shear, Z is the particle's below position with respect to its origin Z_0 and v is the fall speed. However as different size particles have different fall speeds this impacts on the horizontal advection they undergo. Using only two different fall speeds Lo and Passarelli demonstrate graphically how the advection experienced by one set of particles of one size is different than that experienced by a set of larger particles, however there is an overlap between these regions as seen in figure 2.6.

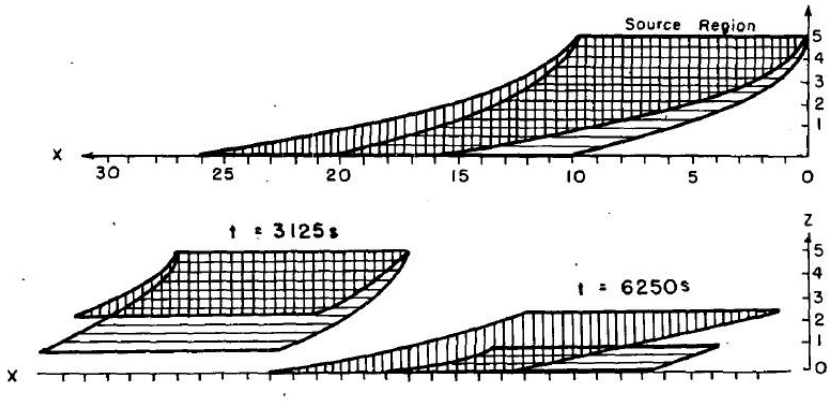

Figure 2.6: Plots of particle trajectories for a steady state line source, top plot, and time-dependent line source, bottom plot, taken from [16, p. 698]

This means that given a steady, finite source there will be a finite region in which horizontal advection can be ignored and the particle growth can be measured as a 1-dimensional problem. Similarly through modelling a source which produces ice particles for only a limited time it can be shown that even if a source is not steady there will always be a region which acts as if the source were in a steady state. Using these two findings Lo and Passarelli surmised that the problem of a horizontally finite, time-dependent source could be reduced to 1-dimension if the aeroplane were to follow these regions, which correspond to a infinite, steady source and no horizontal advection, described. This all presumes finite limits on the fall speeds, which for aggregates [13] suggests is entirely plausible.

Using this modelled behaviour as a guide, Lo and Passarelli proposed a spiral flight path where the fall speed and horizontal drift attempted to match that of the average particle. If the ideal conditions were met, with the diameter of the loops remaining smaller than the area over which the observed atmospheric properties were uniform and the overall condition was as steady as possible, then the flight path is known as the advecting spiral descent (ASD). ASD is designed to be relative to the movement of the air rather than the aircraft's position geographically simplifying the problem as

Lagrangian co-ordinates simplify many problems in fluid dynamics in a way Eulerian co-ordinates would be too cumbersome to do. The data gathered was collected using a Particle Measuring Systems (PMS) 200-Y probe which took 1-dimensional laser images. These were then used to count and size the particles.

The results gathered suggested a size-spectrum approximately of the form:

$$N(D) = N_0 e^{-\lambda D} \tag{2.21}$$

where $N(D)\,\Delta D$ is the concentration of particles in the size range $[D, D + \Delta D]$, N_0 is the intercept and λ the distribution slope. Lo and Passarelli focus on the evolution of parameters N_0 and λ as the aircraft descends along its Lagrangian spiral.

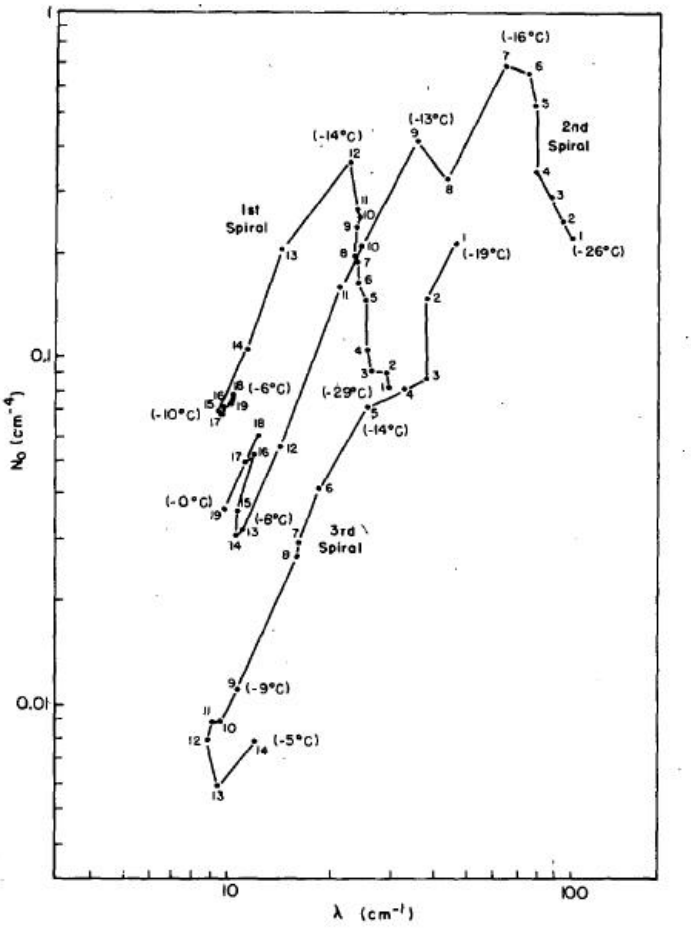

Figure 2.7: N_0-λ evolutions from three separate spirals, taken from [13, p. 702]

As can be seen in figure 2.7, a general pattern of early growth in N_0 and small decreases in λ, changing into the second stage where N_0 decreases as well as λ, before finally stage three is seen where neither N_0 or λ decrease or increase in any significant

way. In figure 2.7 the third spiral is seen to only exhibit behaviour from stages 2 and 3. Lo and Passarelli attribute distinct physical processes to these stages, the first being possibly deposition growth and the second stage aggregation, where the numbers of small particles decrease as they collide and are collided with to produce new larger ones. The third stage is more difficult to attribute, with particle breakup being one possible candidate. This would mean that if a snowflake gets very large it fragments into smaller pieces, stopping the size distribution getting broader, and this could cause λ to stop decreasing at 10cm^{-1}. This last stage is one which is particularly interesting as it cannot be definitively attributed to any particular physical process without significant doubt.

2.3 Other Models of ice aggregation

Many models of ice aggregation have been produced, many building on previous studies and incorporating new advancements in knowledge or techniques.

2.3.1 Passarelli's 1978 model

In 1978 Passarelli [19] attempted to produce a simple analytical model which would approximate both vapour deposition and aggregation. He had noted that, although the methods and technologies involved in gathering observational data on precipitation had been advancing, the interpretation of these results had not been making the same progress. Many of his predecessors and contemporaries had been employing numerical integration of the complex equations that result from the known physical properties of precipitation. However, this is a very cumbersome and expensive technique and often produces overly complex and confused results.

Passarelli assumed that the precipitation was steady and within a vertically heterogeneous cloud and that the size distribution of the ice particles satisfied:

$$n(D) = N_0 e^{-\lambda D} \tag{2.22}$$

as found by Lo and Passarelli [16] from their aircraft measurements. In order to gain solutions for N and λ Passarelli solves the two first-order ordinary differential equations (ODEs) produced by the moment conservation equations for the total mass and the total radar reflectivity, Z. These two moments may be used to derive N_0 and λ, see section 3.4.2, and the total radar reflectivity is proportional to the second moment of the mass distribution as seen in section 3.5. In order to simplify the ODEs enough to solve

them the aggregates are assumed to be spherical so that the mass diameter relationship (2.23) can be used.

$$m = \pi \rho D^3/6 \tag{2.23}$$

where ρ is the density of the individual aggregate. The density is assumed to be constant as a function of D but this is not consistent with observations, for example Locatelli and Hobbs found $m \propto D^2$ which gives $\rho \propto 1/D$ so (2.23) is possibly an oversimplification. The fall speeds of the aggregates are also approximated using a power law, $v = aD^b$ as per Locatelli and Hobbs, where the parameters a and b depend on the type of ice crystals involved in the aggregates. Lastly the precipitation is assumed to be steady and that any vertical flux in the mass and reflectivity is principally due to the fallspeed. This results in N_0 and λ being solved as functions of height below a set level, though if the cloud is assumed to be spatially homogeneous then N_0 and λ are also functions of time and can be compared to previous studies results.

This model was used to predict the size distribution of ice particles as a function of time. Its results were exponential, due to its initial assumption, and therefore appear linear when plotted on a logarithmic-linear scale. When [19, p. 122] Passarelli compared this to contemporary studies which used numerical integration to model raindrop coalescence; its results did not capture all the detail of the full numerical integration, but seemed to give a reasonable approximation. However, this model is an advancement in taking a new look at the techniques and direction that studies of aggregation could take.

2.3.2 Snow Growth Model(SGM)

Mitchell, Huggins and Grubisic detailed their derivation of and the results gained from the SGM in a paper in 2005 [18]. This model was based on analysis started by Passarelli in [19] as discussed above. Once again the several relationships are assumed including:

$$n(D) = N_0 e^{-\lambda D} \tag{2.24}$$

$$m = aD^b \tag{2.25}$$

$$A = \alpha D^\beta \tag{2.26}$$

They also solved the moment conservation equations for the concentration and the total radar reflectivity as part of their derivation of the SGM. The SGM breaks away from many previous studies and takes supersaturation as its input instead of a vertical profile of the ice water content and temperature. The SGM produced results on size

distributions that appear to correspond favourably to the observational data as seen in section 2.2. One interesting analysis from the results was an investigation into the evolution of N_0 and λ. The predicted N_0 and λ relationship evolves into approximately

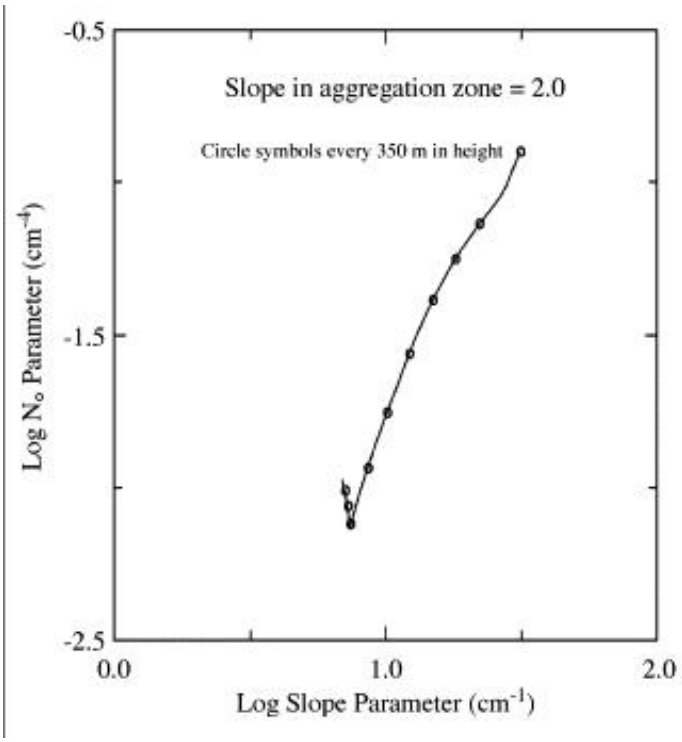

Figure 2.8: Predicted relationship between N_0 and λ by SGM, taken from [18, p. 11]

a straight line with a gradient of 2 in log-log space with N_0 and λ steadily decreasing until the last 3 points. This relationship is similar to the observational findings of Lo and Passarelli [16] which can be seen in figure 2.7. Mitchell et al attribute the power-law relationship, displayed as a straight line in figure 2.8 to the dominance of aggregation in this period. The aggregation is hypothesised to keep broadening the size distribution until the system is dominated by large snowflakes which tend to fall at similar speeds, see section 2.1. The reduced range of fall speeds leads to aggregation eventually becoming negligible. This causes the growth to be dominated by deposition which increases λ steepening the size distribution causing the behaviour in the last 3 plotted points in the bottom left of figure 2.8, which is a similar cut off point to that found by Lo and Passarelli of 10cm^{-1}.

2.3.3 A Monte Carlo Model of aggregation

This project is based on the model produced in work by Westbrook et al [1],[2] and [3] which aimed to model the growth of particles by differential sedimentation in particular, the aggregation of ice crystals in clouds.

In order to simplify the system the following assumptions were made:

1. the cloud is assumed to be dilute, meaning that the mean free path between the collisions of clusters is large compared to the average distance between clusters. This allows the model to ignore spatial correlations and concentrate solely on individual collisions between pairs of clusters.

2. it is assumed that clusters are randomly orientated and that these orientations do not change during collisions or close encounters with another cluster.

3. hydrodynamic interaction does not effect the collision trajectories, so any effect of wakes or boundary layers of a cluster on surrounding clusters are ignored

4. all collisions successfully result in aggregation with a permanent, rigid bond at the point of initial contact

To sample collisions a rate of "close approach" is formulated:

Consider two clusters, i and j, and ascribe to each a radius r_i and r_j; these radii enclose the whole of their respective clusters. Each cluster has a fall speed, v_i and v_j. The rate of close approach is then calculated thus:

$$\Gamma_{ij} = \pi \left(r_i + r_j\right)^2 |v_i - v_j| \tag{2.27}$$

Pairs of clusters are randomly selected with a probability proportional to Γ_{ij}. In this way trajectories in which pairs of particles come close to each other are sampled. Once a pair is selected, one trajectory from all the possible close approaches is chosen at random, and the particles are tracked along this. If a collision occurs then the clusters are aggregated. This method means an unbiased sample of collisions between particles can be gained.

As has been previously shown in section 2.1.2 in [5] Mitchell showed (2.10) that:

$$v \sim \frac{\nu_k}{D} \left(\frac{mD^2 g}{\rho_a \nu_k^2 A}\right)^{\alpha} \tag{2.28}$$

with $0.5 \leq \alpha \leq 1$. Westbrook et al assumed that $A \propto D^2$ based on observational data

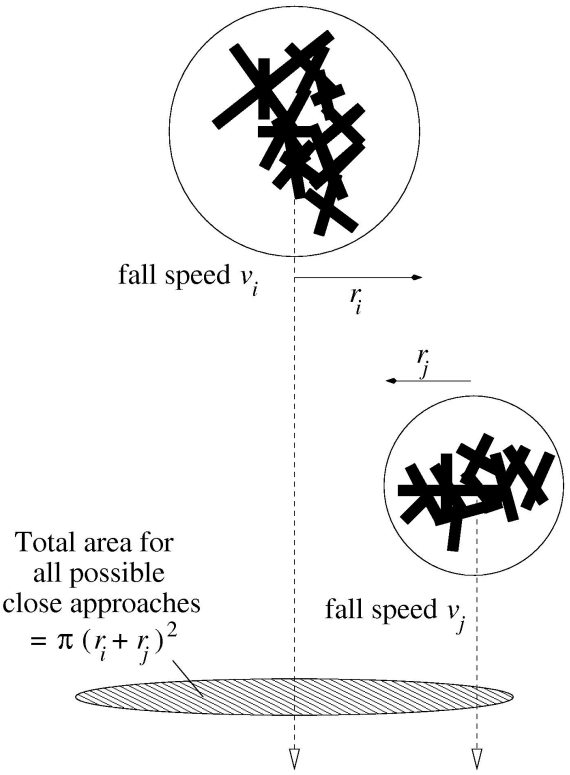

Figure 2.9: To sample collisions a rate of close approach is formulated, this image is taken from [2]

and their results on the fractal dimensions of the aggregates from their simulations. Then substituting this relationship into 2.28 we acquire the equation:

$$v \sim \frac{\nu_k}{r} \left(\frac{mg}{\rho \nu_k^2} \right)^{\alpha} \tag{2.29}$$

In this equation α is an adjustable parameter and $D = 2r$.

Initially all the particles are rods, half with length and mass of unity and the other twice as big and massive. This is so there exists some i and j such that $|v_i - v_j| \neq 0$. Previous studies of aggregation suggest that once sufficient aggregation has occurred the system is insensitive to initial conditions (so having this divide should not impact on the results). From other aggregation models an educated guess can be made that as $m, s \to \infty$ behaviour will satisfy this relationship:

$$n_m(t) = s(t)^{-2} \phi \left[\frac{m}{s(t)} \right] \tag{2.30}$$

$$s(t) = \sum_i m_i^2 / \sum_i m_i$$

Where n_m is the number of clusters of mass m at time t, S is the characteristic cluster mass and ϕ is the rescaled distribution and a function of $m/s\,(t)$. There is some theoretical justification for assuming (2.30) in Van Dongen and Ernst's 1985 study [4] in which they show that (2.30) satisfies the Smoluchowski equation seen below. The scaling function, ϕ, in (2.30) was confirmed using the simulation data and comparison with aircraft measured size distributions. The particle diameter distribution was also measured in these simulations, and found to be approximately exponential, in agreement with the observational data presented in section 2.2.

Other models and studies suggest that the clusters produced by aggregation are likely to be fractal in nature or statistically self-similar. This means that the spatial correlations within the aggregate are similar across a range of different scales, a power law scaling relating them. Though in reality aggregates may differ slightly from this, which can be explained through physical reasoning. As each additional ice crystal that collides and aggregates with the aggregate it forms a protrusion. These protrusions are more efficient at colliding and therefore collecting other ice crystals, which leads to aggregates forming with an open, fractal, structure. The simulation results give a relationship between the mass and radius of the cluster which agrees with the suggestion that the clusters are fractal. As a fractal nature would imply, for any cluster it is found that $m \sim r^{d_f}$ where the fractal dimension d_f is found to be a function of the parameter α as shown in figure 2.10. Note that $d_f \approx 2$ for $\alpha = 1/2$ which corresponds well to experimental data from Locatelli and Hobbs, who estimated $d_f \approx 1.9$, and Heymsfield et al who found $d_f \approx 2.09$.

The Smoluchowski equation is often used to describe cluster-cluster aggregation

$$\frac{dn_k\,(t)}{dt} = \frac{1}{2}\sum_{i+j=k} K_{ij} n_i\,(t)\, n_j\,(t) - \sum_{\infty}^{j=1} K_{kj} n_j\,(t) \tag{2.31}$$

where $n_k\,(t)$ is the number of crystals in the system of mass k at time t and the kernel K is a symmetric matrix where element $K_{i,j}$ governs the rate of aggregation between pairs of clusters of masses i and j. This is a simplification of the simulated system since the aggregation rate is assumed to depend only on particle masses. Then equation (2.27) may be written as:

$$K_{ij} \sim \left| i^{\alpha - 1/d_f} - j^{\alpha - 1/d_f} \right| \left(i^{1/d_f} + j^{1/d_f} \right)^2 \tag{2.32}$$

Analytical solutions to the Smoluchowski equation have only been found for simple cases, where $K_{i,j}$ is constant, $i + j$ or ij. Obviously the $K_{i,j}$ for this model, equation, (2.32) is not of this form and an analytical solution was not found.

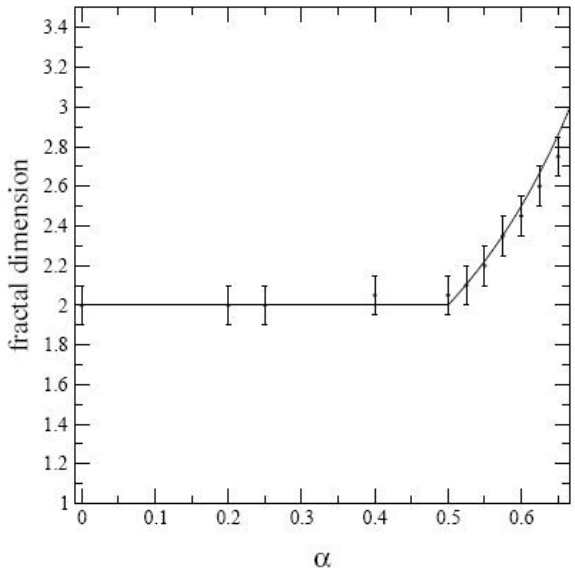

Figure 2.10: The fractal dimension d_f as a function of α, circles are data from the simulation, taken from [2]. Note the physical values of α are between 1/2 and 1

However, substituting (2.30) into the Smoluchowski equation, with the assumption that average cluster mass, s, is large enough relative to the initial conditions, Van dongen and Ernst [4] found some properties of solutions. Assuming $i << j$ the elements of the Kernal scale as:

$$K_{ij} \sim i^{\mu} j^{\nu} \tag{2.33}$$

where $\mu = 0$ and $\nu = \alpha + d_f^{-1}$ for the kernel (2.32).

Westbrook et al then argued that $\nu = 1$ since:

- if $\nu > 1$ then the result is unphysical. The Smoluchowski equation predicts the formation of a big cluster in zero time. For finite system it is expected that a few very large clusters will grow very rapidly, which will then dominate the dynamics and bond with all of the small particles through aggregation. Through this aggregation the smaller particles will fill the gaps in the large particles' structures making them increasingly compact. This causes d_f to increase and ν to subsequently decrease, until the system reaches $\nu \leq 1$

- if $\nu < 1$ then the result is similar with the feedback increasing ν back to 1. In this case more collisions occur between similar size clusters which leads to more open structures. This causes d_f to decrease and therefore ν to increase.

This argument that $\nu = 1$ was found to be a good fit to the simulation data as shown by the solid line in figure 2.10. For inertial flow, if $\alpha = 1/2$ then $d_f = 2$, which is in

agreement with observational studies including Locatelli and Hobbs [13].

Chapter 3

A refined Monte Carlo model of aggregation

The new results presented here were produced using a modified version of the Westbrook et al Monte Carlo model described in section 2.3.3. The model attempts to simulate the aggregation of hexagonal plate ice crystals in a deep stratiform ice cloud with an improved representation of the aggregate fall speed using equation (2.19). Key variables are defined by the user:

- the initial number of crystals, n.
- the aspect ratio, $t/2a$, of those crystals, see figure 3.1 where t is the plate thickness and $2a$ is the diameter across its hexagonal face.
- the finishing diameter, D_f, when the average diameter of all the particles within the simulation reaches this number the simulation finishes.
- the initial crystal size, t, half the monomers are chosen to have this size, the other half are twice as big.
- a random seed, to allow the user to produce 'ensembles' of different simulations with the same parameters.
- the wobble, W, the degrees by which the crystals will be able to tilt from the horizontal within the simulation. Experimental data [32] shows that planar crystals tend to be orientated with their major axes horizontal with a small amount of wobble, dependent on the Reynolds number. Here it is assumed that the crystal orientation is uniformly distributed between $0° - 10°$.

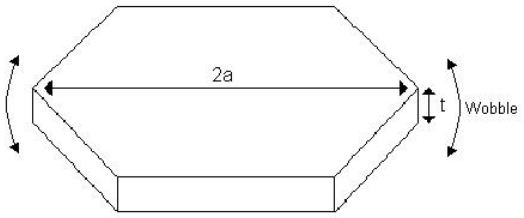

Figure 3.1: Diagram of parameters

Other variables are also adjustable by the user however they pertain to more specific measurements and outputs. We assume that the aggregates are randomly oriented as they have little symmetry and there is little observational evidence either way.

3.1 Mass Diameter relationships

As discussed in Chapter 2 observational studies are used in the process of assessing a model's success in reproducing reality. The relationship between the mass and the diameter of aggregates frequently forms a fundamental part of these studies. Most observations suggest a power-law relationship $m \propto D^{d_f}$ where d_f is the fractal dimension as discussed in section 2.3.3.

In order to gauge how the model is predicting this relationship each aggregate is assigned to a bin according to its diameter after a simulation has run. The number of particles in each bin and each bin's collective mass is then ascertained. The model then outputs this data cataloguing, for each bin, the lowest possible diameter for aggregates in the bin with the average mass of the aggregates in the bin, using the collective mass and the number of particles in the calculation. From this we can observe whether the model is reproducing the observed mass-diameter power-law relationship.

Figures 3.2 and 3.3 show the relationship between the mass and diameter. Firstly figure 3.2, where the same parameter values are observed with only the random seeds changed, which provides a sample of the same outcomes for the one set of parameter values or for one 'cloud'. Secondly, in 3.3 different parameter values are employed to give an idea of the sensitivity of the mass-diameter relationship, and consequently the model, to the different parameters. By looking at both these ways of 'randomising' the results, despite the obvious noise in the plots, we can hopefully be more confident in the universality of the results. In order to really judge the relationships being produced here it is best to look at the results on logarithmic scales in log-log space.

As can be seen in the loglog plots in Figures 3.4 and 3.5 the relationship between mass

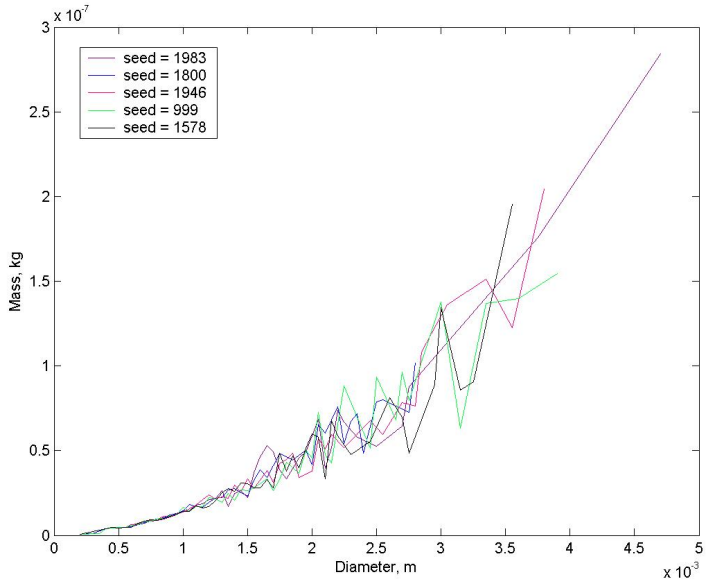

Figure 3.2: Plot of Mass-Diameter relationship for 5 runs with different random seeds

and diameter appears to be approximately $m = aD^{d_f}$ where $d_f \approx 2$. This relationship agrees many of physical observations and studies. In Locatelli and Hobbs [13] it is estimated that $d_f = 1.9$ from data extrapolated from sample aggregates of plates, side planes, bullets and columns in ground based observations. Aircraft observations by Heymsfield et al [11] yielded $d_f = 2.04$ for aggregates of bullet rosette crystals in cirrus clouds and $d_f = 2.08$ for aggregate of side plane crystals. Mitchell [5] gives estimates of d_f between 2.1 and 2.2, depending on the individual crystal types in the aggregation. This agreement lends support to the model and its close approximation to physical reality, at least in this fundamental area.

This result also agrees with C.D.Westbrook's findings in [1], [2] and [3] using the unmodified model. Westbrook found an approximate relationship of $m \propto D^{2.05\pm0.1}$ for his simulations and $d_f = 2$ from analysis of the Smoluchowski equations for $\alpha = \frac{1}{2}$. In these studies the approximately quadratic relationship is discussed as a possible result of the hydrodynamic power law for the particle fall speeds as discussed in section 2.3.3. Those calculations used the less realistic fall speed calculations based on equation (2.17). The new model presented here uses the full fall speed relationship (2.19) allowing the particles to span a range of hydrodynamic regimes, and also explicitly includes a calculation of the projected area rather than simply assuming $A \propto D^2$ as Westbrook et al did. This gives us more confidence that we are capturing the physics of the collisions correctly. Therefore, only the larger particles' fall speeds are calculated using

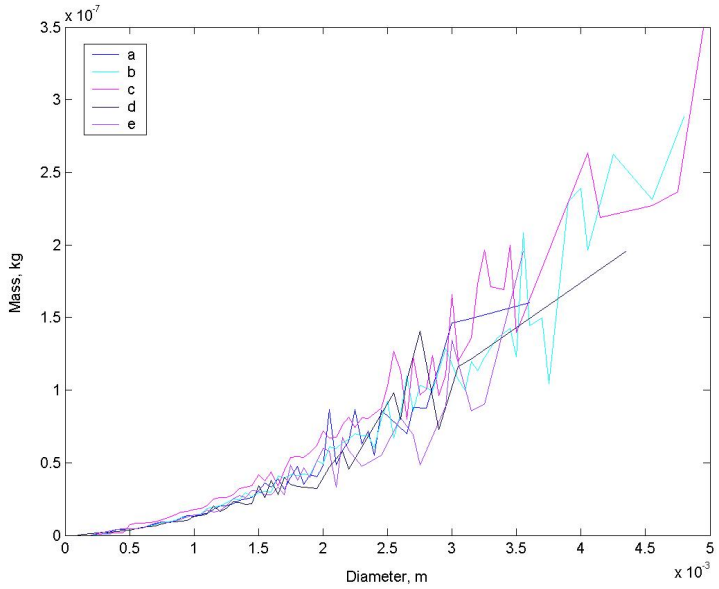

Figure 3.3: Mass-diameter relationships from runs with different values for parameters $(n, t/2a, D_f, t, W, seed)$ listed run a to e: $(5000, 0.1, 605, 20e-6, 10, 1948)$, $(10000, 0.1, 800, 20e-6, 10, 1983)$, $(7500, 0.1, 750, 25e-6, 10, 1946)$, $(5000, 0.15, 500, 20e-6, 10, 1911)$, $(2500, 0.1, 650, 20e-6, 10, 1578)$.

a similar equation to [1]. Yet the mass-diameter relationship still remains approximately quadratic, this could suggest that this relationship, or at least the methods by which it is currently studied, is biased towards the larger particles. It is also possible that the aggregation is largely controlled by the larger crystals capturing the smaller crystals so the fall speeds of the larger crystals are more influential and control d_f.

3.2 Velocity Diameter Relationships

The fall speed, in both observation and modeling, holds a significant amount of interest in modern research into aggregation and many theories are being proposed, tested or modified in the pursuit of a better understanding of reality. In Mitchell and Heymsfield's [9, p.1642] paper and Mitchell et al's [18] paper they predict that for all aggregates with large diameters the fall speeds will not differ greatly. This reduction in the dispersion of fall speeds for larger aggregates is then advocated by Mitchell and Heymsfield as a reason why aggregation at larger dimensions (approximately $\geq$ 2mm) may occur at increasingly negligible rates, in an effort to explain the observations of Lo and Passrelli in section 2.2 where they found that the size distributions did not broaden further than $\lambda = 10\text{cm}^{-1}$.

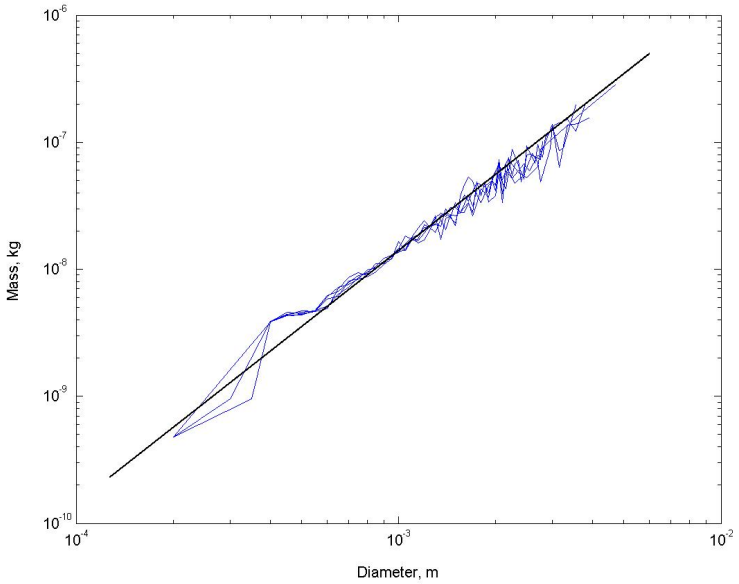

Figure 3.4: Plot of Mass-Diameter relationship from Figure 3.2 on logarithmic scales, the solid black line indicates a $m \propto D^2$ relationship

The model uses a similar technique as that used to output the necessary information for the mass-diameter relationship. The data from aggregates is allotted to bins according to its diameter and the average velocity for each bin is calculated.

It can be seen in figure 3.6 that the mean velocity for each diameter bin does conform in general, excluding noise, to the theory that Mitchell and Heymsfield proposed in [9] and Mitchell et al referenced in [18] with the fall speed flattening out as D increases past 1mm. However, just looking at the mean velocity is not the whole picture.

Figures 3.7 and 3.8 show the detailed situation, displaying the velocity against the diameter of each aggregate in the simulation. These figures are just a selection of what the model consistently produced, which demonstrate that, when the simulation is run for any significant length, the larger aggregates, with diameters greater than 2mm, have a considerable amount of dispersion in their fall speeds for a given particle diameter. Similar results can be seen in plots of Locatelli and Hobb's observational data [13]. Although the fall speed equations used in the model are those used by Mitchell and Heymsfield, the model applies them more realistically than in [9]. In [9] area- and mass-diameter power-law relationships are assumed which are 1-to-1 functions and predetermined, whereas the model uses each aggregate's individual area and mass, and of course 'every snowflake is different'. The new model presented here is believed to be more physically realistic in this respect, by allowing the individual geometry of each

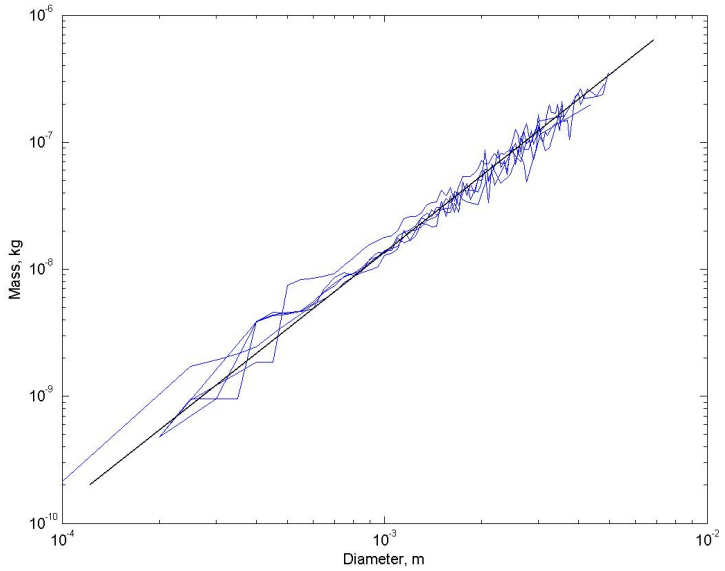

Figure 3.5: Mass-Diameter relationships from figure 3.3 in log-log space, the solid black line indicates a $m \propto D^2$ relationship

aggregate to influence these parameters and through them the fall speeds.

As there is less data for the higher diameters a fairer measurement needs to be employed to estimate the variation of the velocities as a function of aggregate diameter.

Figures 3.9 and 3.10 display the mean and standard deviation of the velocities for each bin against the diameter for runs with the same parameters as figures 3.7 and 3.8. The standard deviation is calculated for each bin using:

$$\sigma = \sqrt{\frac{1}{n_r} \sum_{i=1}^{n_r} (v_i - \bar{v})} \tag{3.1}$$

where n_r is the number of aggregates in the bin, $v_1 \ldots v_{n_r}$ are the individual velocities of the aggregates assigned to this bin and $\bar{v}$ is the mean velocity for this bin. As the standard deviation measures the variation taking into consideration the number of points in each dataset it is a good measure to use in this situation, ignoring those bins with only one value.

There does appear to be some decrease in the standard deviation from $\approx 0.4\text{ms}^{-1}$ variation at $500\mu m$ to $\approx 0.2\text{ms}^{-1}$ at 2mm, however, this is still significant and represents 18% of the mean value. These results suggest that the natural variability in aggregates shape could lead to enhanced aggregation rates, a factor which was neglected in Mitchell and Heymsfield's analysis, and suggests that, in this model at least, any reduction in

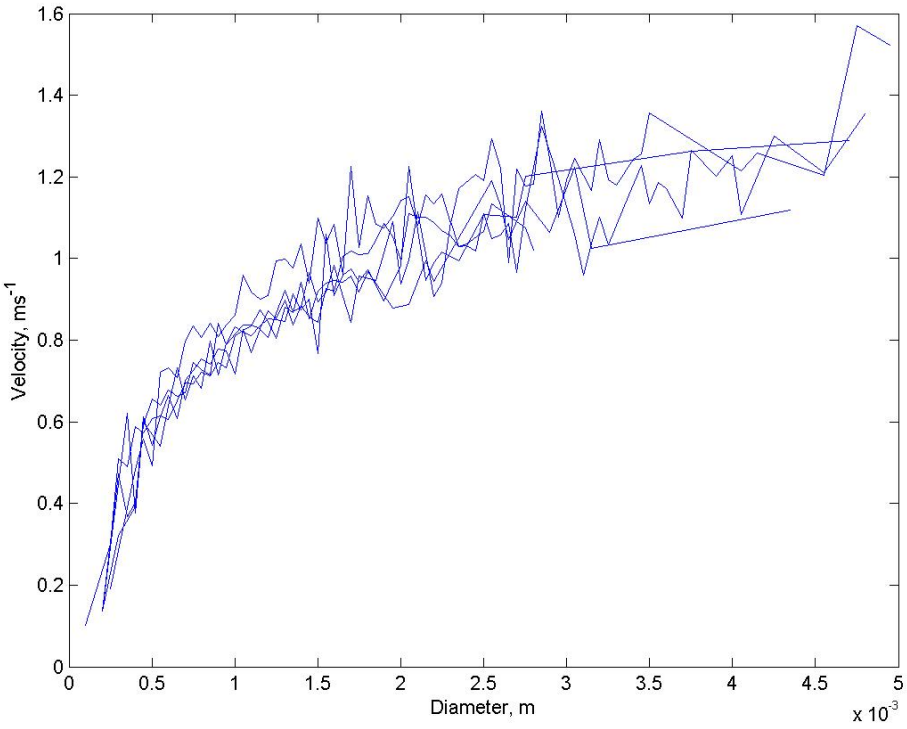

Figure 3.6: Mean velocity-Diameter plots for varied runs, using the same parameter values as figure 3.3

aggregation when aggregates become large is not due to them all having the same fall speeds.

3.3 Diameter - time relationship

Throughout the simulation, every time an aggregation occurs the model calculates the average diameter, using all particles within the simulation, and then outputs this with the time. Time within the model is determined for each close approach using equation (2.27) and the number of clusters left in the simulation.

The average diameter continues to grow throughout the simulation. The points in the plot corresponding to the lowest diameters can be ignored as they correspond to the initial monomers and as such are not necessarily physically relevant. From figure 3.11 it appears that growth generally increases in a steady manner. The apparent 'jumps' in time are a product of a finite number of particles in the simulation and a close approach occurring for a pair of clusters for which the corresponding probability (2.27) was low.

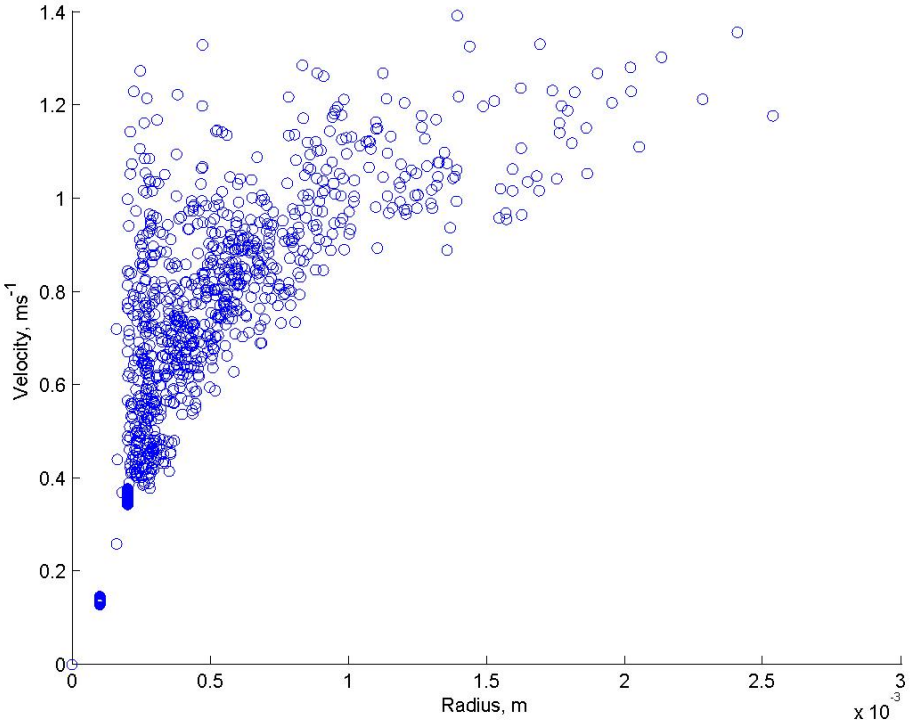

Figure 3.7: Plot of velocity against mass for individual aggregates, with $n = 10000$, $t/2a = 0.1$, $D_f = 800$ and $t = 20x10^{-6}$

3.4 N_0 - λ

The parameters N_0 and λ are often studied and are used to describe the relationship between the concentration and diameter as has been previously introduced in 2.21. It is the evolution of these parameters throughout aggregation and therefore our simulation which is of particular interest. Lo and Passarelli [16] separated the evolution into three stages discussed in 2.2. Of these sections it is the third that is of the most interest as it is not yet widely accepted as attributable to any particular mechanism.

It is necessary to attempt to estimate the values of N_0 and λ from the data in the simulation as direct calculation is not possible. This was first attempted by programming the model to output the size distribution at given points during the simulation.

The example of the evolution of size distribution from the model in figure 3.12 is typical. Though the size distribution could be exponential for large D, as predicted by the well-used assumption $n(D) = N_0 e^{-\lambda}$, the noise in the data in these plots overwhelmed any possible underlying relationship making it impractical to estimate N_0 and λ, or indeed to reliably confirm that $n(D)$ was exponential. Attempts using wider diameter

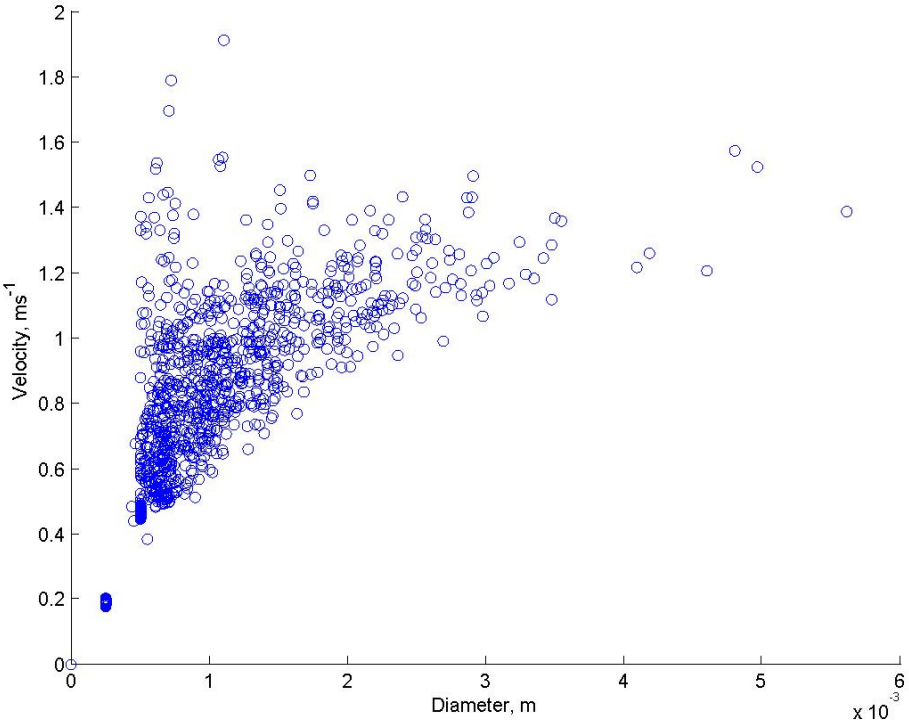

Figure 3.8: Plot of velocity against mass for individual aggregate, with $n = 7500$, $t/2a = 0.1$, $D_f = 750$ and $t = 25x10^{-6}$

bins used to gather the data in the model were unsuccessful in reducing the amount of noise to the point where a discernible relationship was apparent.

3.4.1 Moments

The next method attempted, with the hope of overcoming the problem of noise, involved the calculation of moments from the data. The i^{th} absolute moment M_n of a probability function $f(x)$ about a point a is calculated thus:

$$M_i = \int_{-\infty}^{\infty} |x - a|^i f(x)\, dx \tag{3.2}$$

For the relationship $N(D) = N_0 e^{-\gamma D}$, D replaces x, $a = 0$ and $N(D)$ replaces $f(x)$ in 3.2 and as N is output from the model as a positive discrete function the integration becomes a summation over all the bins with a lower limit of 0:

$$M_i = \sum_{0}^{\infty} D^i N(D)\, \Delta x \tag{3.3}$$

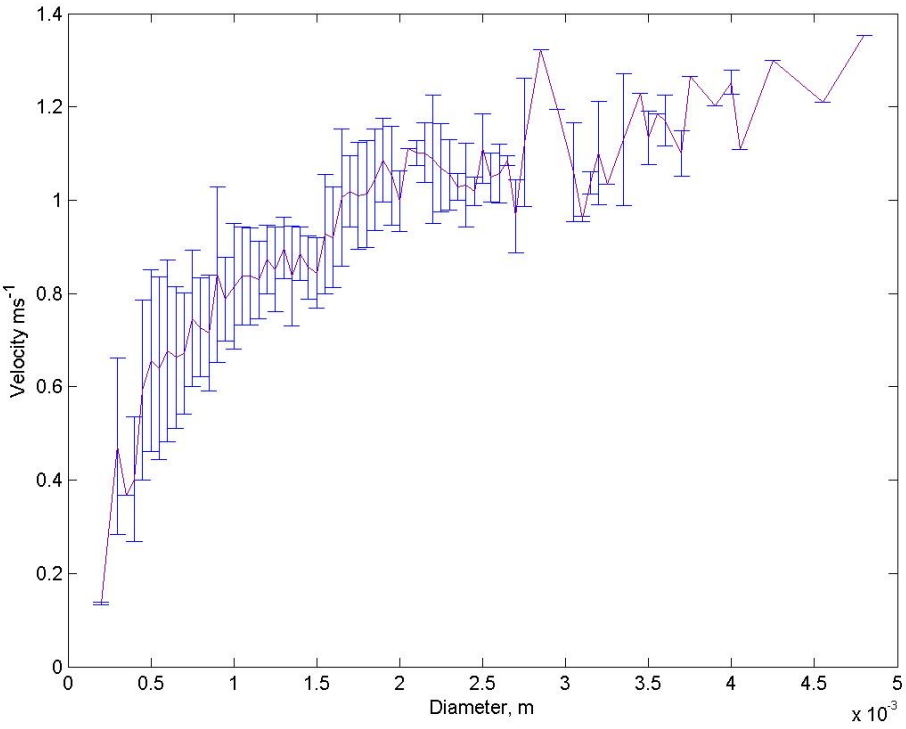

Figure 3.9: Mean and Standard deviation of velocity, with $n = 10000$, $t/2a = 0.1$, $D_f = 800$ and $t = 20x10^{-6}$

However the M_i can also be written as:

$$M_i = N_0 \int_0^\infty D^i exp\left(-\lambda D\right) dD = N_0 \frac{\Gamma\left(i+1\right)}{\lambda^{i+1}} \tag{3.4}$$

By equating 3.3 and 3.4 and using $\Gamma\left(i\right) = (i-1)!$ equations to estimate λ and N_0 are created applicable for any i in the natural numbers:

$$\lambda = \left(i+1\right) \frac{M_i}{M_{i+1}} \tag{3.5}$$

$$N_0 = \frac{M_i \lambda^{i+1}}{i!} \tag{3.6}$$

The model output λ and N_0 for each individual moment and an average estimate calculated from these for predetermined points in the simulation. However, initial results were not very successful and appeared to give very little correlation. This was possibly due to the inclusion of the lower order moments, which are in their calculation weighted towards the smaller diameter end of the spectrum and the monomers. As this part of

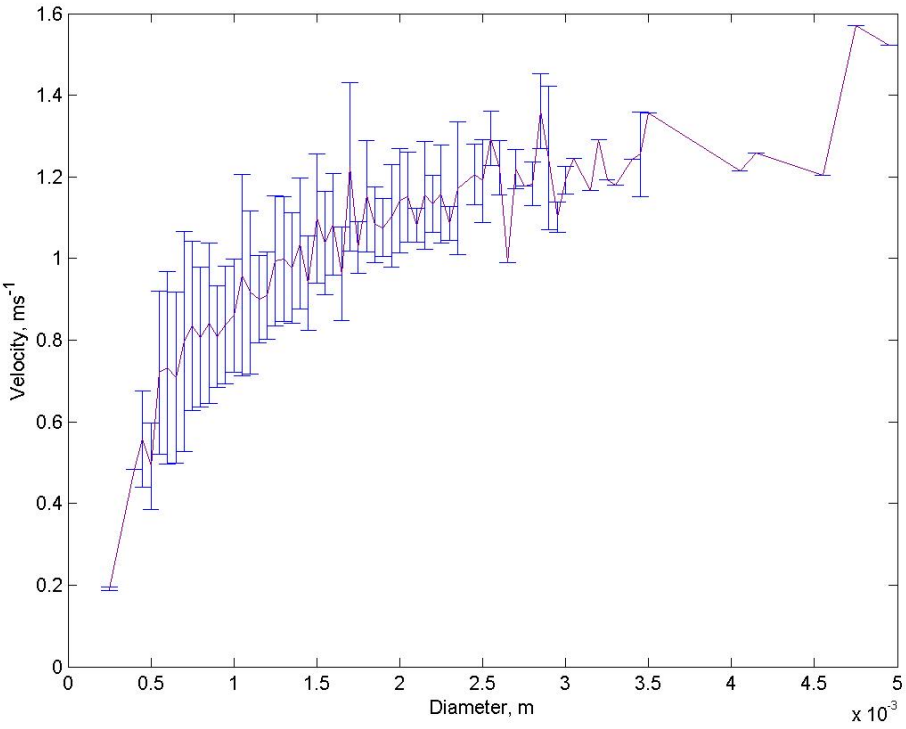

Figure 3.10: Mean and Standard Deviation of velocity, with $n = 7500$, $t/2a = 0.1$, $D_f = 750$ and $t = 25x10^{-6}$

the simulation is not yet independent of its initial conditions it is not appropriate or physically correct to lend such weight to this data. So the model was made to work only on medium order moments:

In Figure 3.13 the evolutions of N_0 and λ in general agree with the second stage noted by Lo and Passarelli [16], that of a mutual reduction. Some of the plots seem to exhibit behaviour towards the end that may be consistent with stage 3 though it occurs at slightly higher values with most studies placing it at around 10cm^{-1}. The lack of consistency between the different derived N_0-λ curves in figure 3.13 may suggest that either the size distribution was so noisy as to strongly effect the moments used, or that deviations from the assumed exponential shape $N = N_0 e^{-\lambda D}$ biased the estimates of N_0 and λ.

3.4.2 Integrating the size distribution

Here we will investigate an alternative approach to estimating N_0 and λ.

Many studies and models have been based on the assumption that the size distribu-

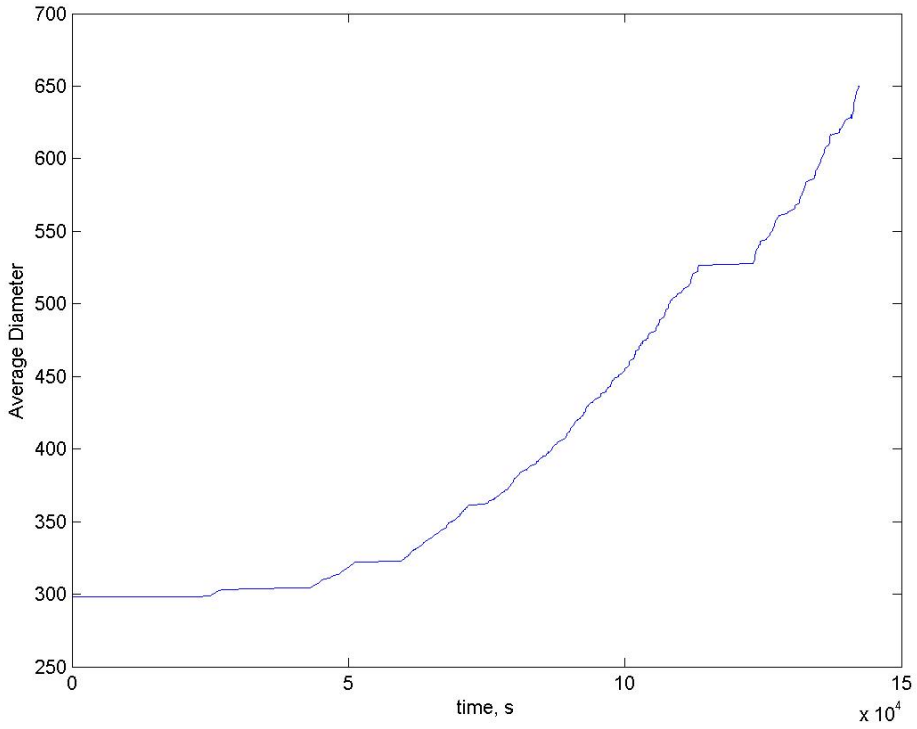

Figure 3.11: A typical plot of average Diameter against time produced by the model

tion satisfies the relationship:

$$N(D) = N_0 e^{-\lambda D} \tag{3.7}$$

where $N(D)\,\Delta D$ is the concentration of particles in the size range $[D, D + \Delta D]$, N_0 is the intercept and λ the distribution slope. However, in attempts to measure N_0 and λ using the plots of the size distribution, output at allocated times during the simulation, was not entirely successful due to the amount of noise in the plot, see figure 3.12. However if equation (3.7) was integrated from the largest size downwards, an exponential relationship would still be retained as seen in (3.8):

$$I = \int_D^\infty N(D')\,dD' = \int_D^\infty N_0 e^{-\lambda D'} dD' = /\frac{N_0}{\lambda} e^{-\lambda D} \tag{3.8}$$

Once again, at appointed times in the simulation, the model allocates the aggregates to bins determined by their diameter and the number of aggregates, or frequency, in each bin is recorded. As this method of obtaining the size distribution results in a discrete, rather than a continuous, function the integration in (3.8) becomes a sum. For each bin, beginning with the bin corresponding to the largest recorded diameter, the integrated

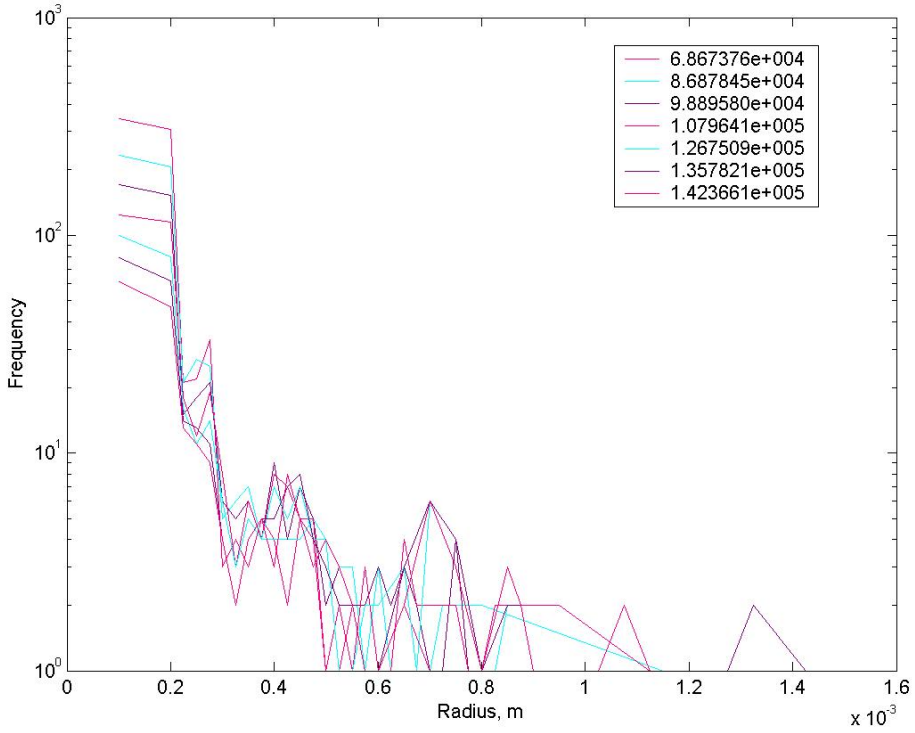

Figure 3.12: Size Distribution evolution example in log-linear space

size distribution, I, is calculated by summing the frequency of current bin to the I of its neighbouring bin. This results in the plot show that much of the noise seen in figure 3.12 is eliminated; this is the advantage of integration where the noise is accumulated and, to an extent, cancels itself out. The resulting curves in figure 3.14 show that $I(D)$ is approximately exponential which confirms that $n(D)$ is also approximately exponential, an important relationship for the model to capture and reproduce.

Figure 3.14 is plotted in $log_{10}I$-D space which means that the relationship, using logarithmic rules, becomes:

$$\frac{log_{10}I}{log_{10}e} = \frac{log_{10}\frac{N_0}{\lambda}}{log_{10}e} + log_e e^{-\lambda D} \tag{3.9}$$

$$log_{10}I = log_{10}N_0 - log10\lambda - (log_{10}e)\,\lambda D \tag{3.10}$$

Therefore, a best fit can be used to estimate the gradient from each slope, so it can be ascribed to $-(log_{10}e)\,\lambda$, the intercept can also be estimated and it is $log_{10}N_0 - log10\lambda$.

Figure 3.15 shows us a relationship between N_0 and λ which, for higher values of N_0 and λ, is as expected and represents the 'stage 2' which Lo and Passarelli observed

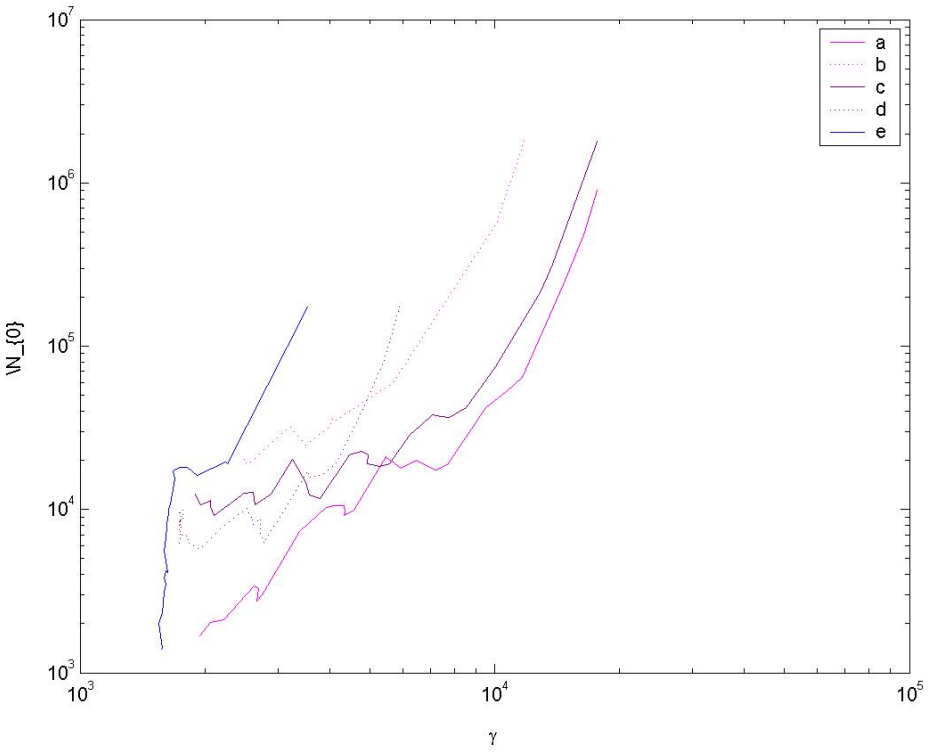

Figure 3.13: Evolutions of N_0 and λ estimated in different runs using moments 4 to 9

[16] as it is discussed in section 2.2. However unlike the results produced by Mitchell et al the relationship continues to values of $\lambda < 10\text{cm}^{-1} = 1000\text{m}^{-1}$. Mitchell et al's prediction for the change in the N_0 and λ relationship was based on the similarity of the velocities of larger particles leading to a reduction in aggregation. This new model, as had been suggested in 3.2, shows evidence that possibly contradicts Mitchell et al's predictions and suggest that aggregation can in principle continue to broaden the size distribution even when the particles are large.

3.4.3 Other Studies

There are many competing theories on the relationship between N_0 and γ particularly what occurs at around $\lambda = 10cm^{-1}$ and what drives this behaviour. Lo and Passarelli [16] examine the behaviour around $\lambda = 10cm^{-1}$ in their observations to find all cease to evolve, indicating that the a balance within the size distribution has occurred with smaller particles that aggregate being replaced and the larger particles that aggregation is producing are reducing in number. Lo and Passarelli propose that this behaviour is consistent with a mechanism of the largest snowflakes breaking up on impact, which is a

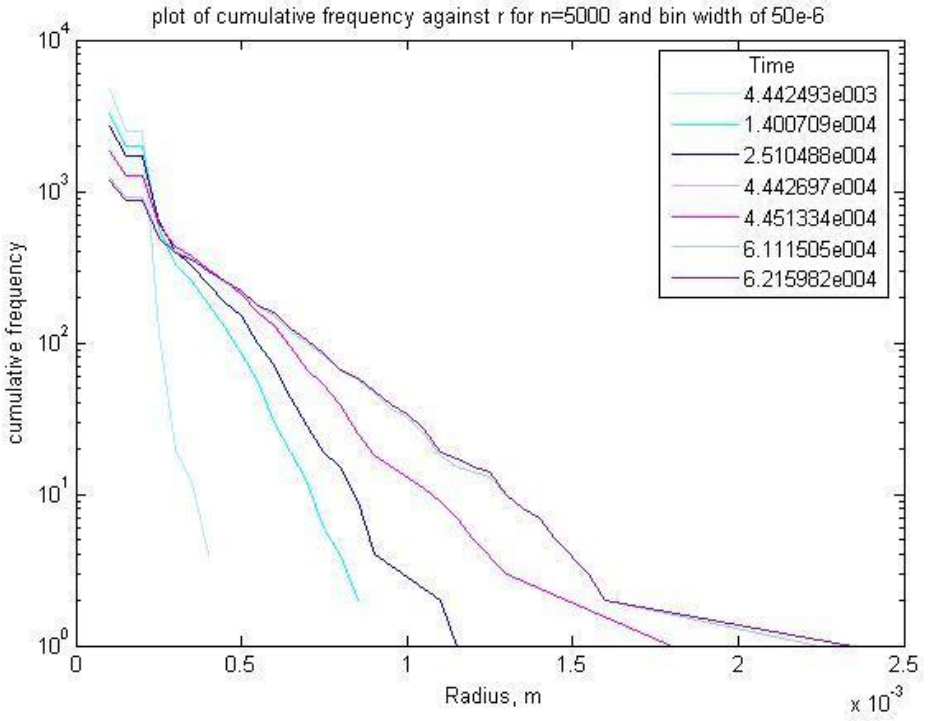

Figure 3.14: Evolution of cumulative size distribution

mechanism not included in this new model, though they concede that it could potentially be the product of instrument-artifact.

Mitchell et al. [18], as discussed in section 2.3.2, used results from their Snow Growth Model to attempt to validate the Mitchell and Heymsfield hypothesis, suggesting that the change between the power-law relationship seen in stage 2 and the more static relationship in stage 3 was due to aggregation ceasing to be the dominant growth mechanism for the ice crystals. This would mean that the velocities of larger ice crystals would have to be very similar making the possibility of collision and therefore aggregation negligible. However, the present study has shown that there may still be significant dispersion in the fall speeds of larger ice crystals, see section 3.2.

More recently studies have emerged that support an instrument-based explanation for the behaviour of N_0 and γ. Korolev and Isaac's 2004 study [21] and Field et al's 2006 study [22] both investigate the hypothesis that Optical Array Probes (OAP) and High Volume Precipitation Spectrometers (HVPS) have been providing incorrect data for observational studies due to the shattering of particles on the instruments. When a large particle shatters on the probe inlet, its contribution to $n(D)$ is lost but the smaller pieces of it that remain could be counted by the optical probes. In many earlier observational studies this process was not known of so any readings from the shattered

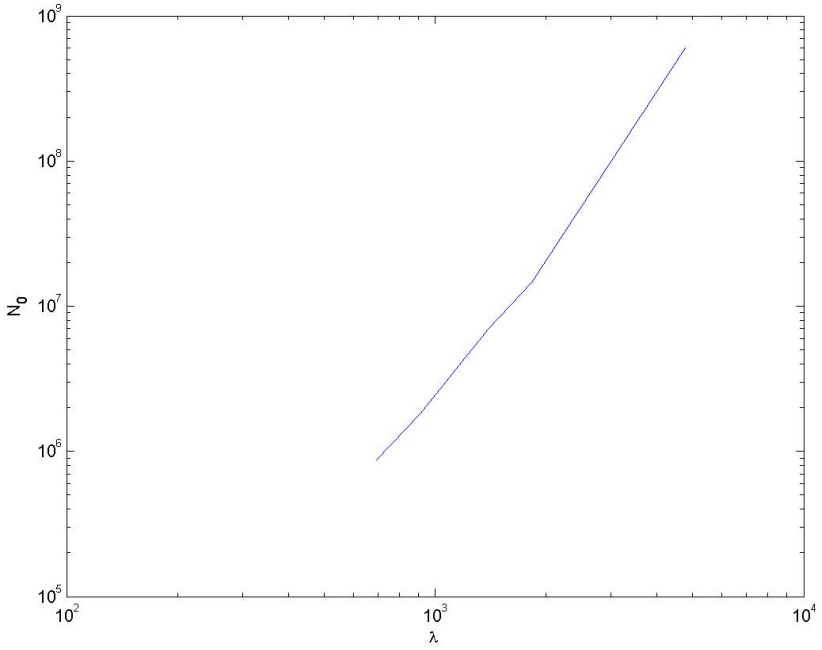

Figure 3.15: Using results from figure 3.14 and basic fitting produces this N_0-λ relationship

particles would not to be rejected from a study and it could cause there to be a skew in the data, especially further into the aggregation process or equivalently lower down the cloud where the particles are larger. This could possibly account for the behaviour seen later on in the evolution of the N_0-γ plot, as suggested by Heymsfield et al in [34], who argues the true values of λ continue to decrease past $\approx 10\text{cm}^{-1}$.

3.5 Calculating Radar Observables

Another method of measurement frequently employed in Meteorology is radar. Doppler radar is sensitive to the concentration, size, fall speed and types of hydrometers including ice crystals, within clouds. Radars emit pulses of radiation, typically between 3mm and 10cm in wavelength, and Rayleigh scattering by the snowflakes leads to some of the wave being reflected back, and the intensity and time taken are measured by the radar. An example time series from a vertically pointing 8.6mm radar at the Chilbolton observatory in Hampshire is shown in figure 3.16 and the radar is pictured in figure 3.17. It is possible to see a thick stratiform ice cloud with rain at the ground and the cloud top at 8000m to 9000m for the time period studied in this dissertation, 0300-0800 hours.

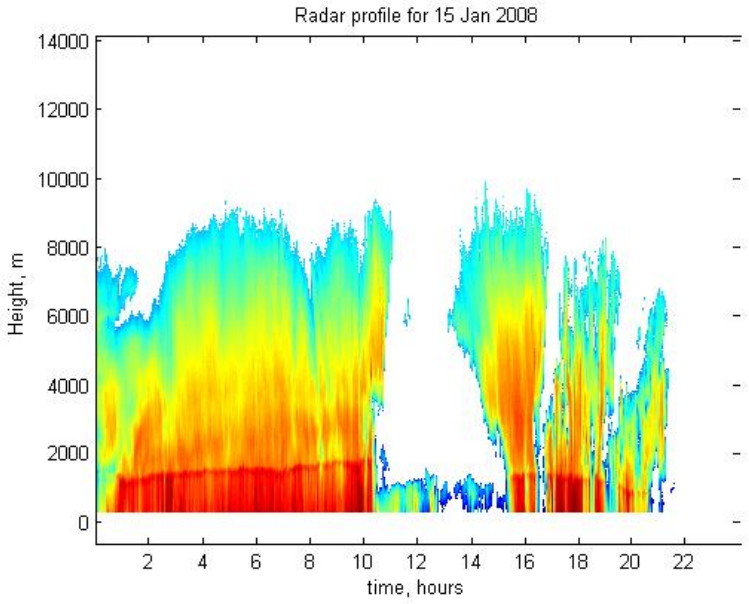

Figure 3.16: Time series from data taken using 8.6mm radar at Chilbolton observatory on 15.01.08

It is of the reflectivity that we are most concerned, with higher values of reflectivity lower in the cloud corresponding to the larger hydrometers. Reflectivity is measureed by assessing the intensity of the returned pulses and is expressed in dBZ, a logarithmic unit. For Rayleigh scattering, the reflectivity can be related to the data obtained from the model as:

$$dBZ = 10\log_{10} M_2 + A \tag{3.11}$$

where M_2 is the second moment of the particles mass distribution, and as such is

Figure 3.17: Image of the Galileo (left) and Copernicus (right) radars at Chilbolton observatory in Hampshire. The data in this study is taken from Copernicus, the 8.6mm radar. This image is taken from [37]

weighted towards the larger snowflakes, and A is a constant calculated by:

$$10\log_{10}\left(\frac{36\left|K_{ice}\right|^2}{0.93\pi^2\rho_{ice}^2}\right)$$

as seen in [35]. The Doppler velocity, v_d, is also measured which is equivalent to the average speed that the particles are moving towards the radar.

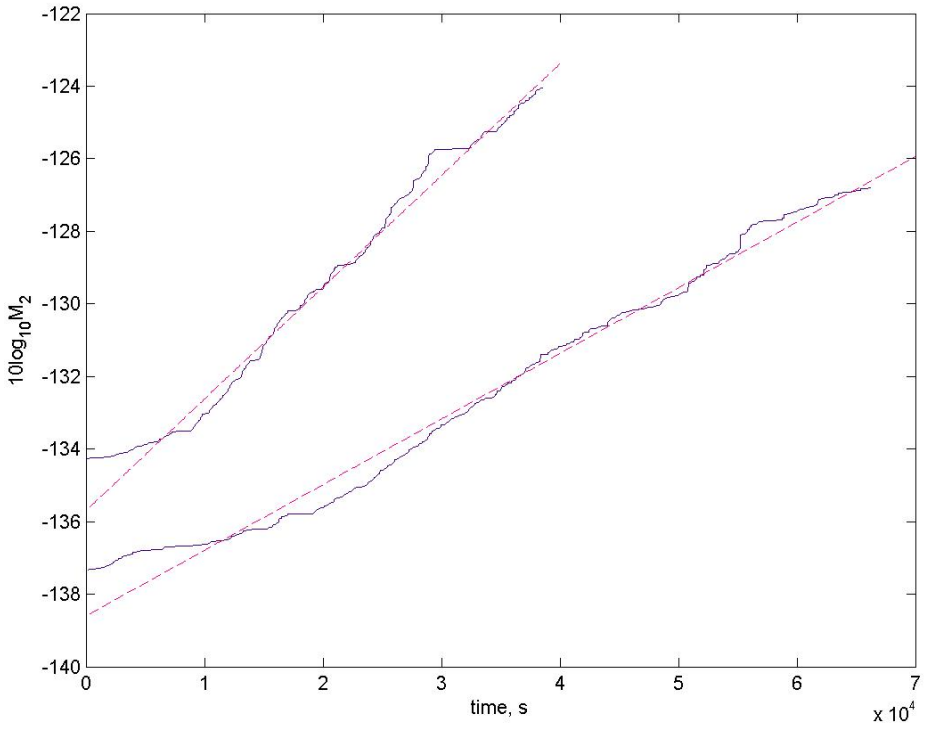

Figure 3.18: Plot $10log_{10}M_2$ against time for different conditions, the pink dashed, line represents a linear fit of the relationship

Comparison of the general form of the results with radar data can be undertaken, however, a numerical comparison of the absolute dBZ values would be meaningless due to the unknown scale of ice production at the cloud top. The similarity in the shape of these plots supports the fact that the initial conditions on the ice crystals in the model do not affect the result in figure 3.18 and we observe that the second moment of the mass distribution grows approximately exponentially with time.

Figure 3.19 is constructed by the method outlined in Westbrook et al's paper [35]. The highest data point with a measurable reflectivity in the vertical profile is taken to be the height of the cloud top, h_{top}, which is presumably where the ice is formed. From

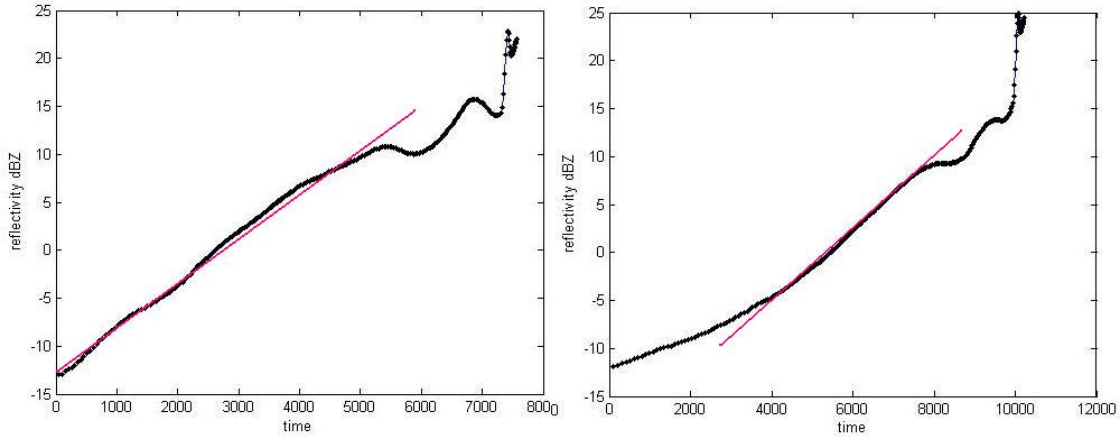

Figure 3.19: Radar data for reflectivity with fitted linear relationships (pink), measured 15 January 2008 at 4-4.30 (right) and 4.30-5.30 (left), the melting layer is shown at approximately 7250 seconds (left) 9500(right)

here the ice grows and falls, and the average velocity of the particles through the vertical profile is known from the Doppler velocity, v_d measurements. From these the time a particle has taken to get to a particular height, h, can be calculated thus:

$$t = \int_h^{h_{top}} v_d^{-1} dh \tag{3.12}$$

as per equation 2 of [35], this represents an 'average' fall time for the ice particles. Then dBZ is plotted as a function of t.

Both figures 3.18 and 3.19 show an approximately linear relationship between dBZ or $10log_{10}M_2$ and time indicating that the model is capturing the evolution of the ice aggregation in a realistic way. The jump in reflectivity towards the end of the plots in 3.19 represents the point where the ice crystals are melting and as such won't be reproduced by the model. These results once again support the model as a close approximation to reality, although we note some non-exponential structure in figure 3.19. This non-exponential structure may be associated with other physical processes or feedbacks in the cloud like evaporation, riming or deposition that is not included in this new model. The data from the radar has also had to be averaged over time periods of $\frac{1}{2} - 1$ hours to account for the fact that the cloud is not perfectly homogeneous in the horizontal.

Chapter 4

Investigating the influence of velocity dispersion on aggregation

Two other papers have considered the effects of velocity dispersion on aggregation, the first by Passarelli and Srivastava [38] and the second by Sasyo and Matsuo [39]. However, the new modified Monte Carlo model employed in this dissertation has the advantage over these previous studies as it explicitly resolves the shape of individual particles. Like many previous studies, including Passarelli, as seen in section 2.3.1 and Mitchell et al, as discussed in section 2.3.2, these two studies both assumed the existence of a 1-to-1 relationship between particle mass and diameter. They did however use an assumed probability distribution of different fall speeds as a function of D in the calculation of the collision rate. This produced a dispersion in the velocity that was uniform around the mean. Both studies found that the effect of variability in the fall speeds was to increase the growth rate significantly. Passarelli and Srivastava also discovered that the size spectrum broadens and reflectivity increased.

Mitchell et al stated in their 2006 paper [18] that their results supported a hypothesis that the rate of aggregation slows to such a negligible rate when a particle's diameter gets large that it appears to stop. This has been previously discussed in sections 2.3.2 and 3.2. It is based on the theory that for large particles the dispersion of fall speeds is very small and as such $K_{i,j} \propto |v_i - v_j| (D_i + D_j)^2$, which corresponds to the rate of aggregation between two particles i and j, is very small. However, results from this model have shown the evidence to support the idea that the dispersion between fall speeds for large particles is not negligible, see figures 3.7 - 3.10. For large particles however, $(D_i + D_j)^2$ is large and so only a small dispersion in the velocities may be needed, thus $|v_i - v_j| \neq 0$, for a reasonable rate of aggregation. Therefore it is necessary to investigate whether calculating the fall speeds of individual particles based on geometry, and therefore not

stopping aggregation for larger particles as is done in the model, produces very different results than if a simpler relationship was used to calculate the fall speed as Mitchell et al did in [18].

4.1 Comparison with a simplified velocity-mass relationship

There are two ways in which the calculation of a particle's velocity can be simplified to the level used in many studies. The first is to use a simple power law of the form $v = am^b$ and the second is to use power laws for the mass-radius and area-radius relationships which can be substituted into the velocity equations already in use in the model, thereby eliminating any dependence of the velocity on an individual particle's geometry.

In order to produce a 1-to-1 velocity-mass relationship, against which the model can be tested, the full simulation is run with a given set of conditions and the velocities and masses of each particle output. This allows a best fit to be found and from this a velocity-mass relationship for the conditions can be established. The simpler model, S1, is then produced as exactly the same as the original model but with all velocity calculations replaced by a simple function of mass.

The 1-1, power-law, mass-radius and area-radius relationships are found using a similar method. The second simpler model, S2, is produced by inputting dummy variables for the radius and area as a function of mass into the fall speed equation, (2.19). The dummy variables are constructed using the power law relationships for mass against radius and area against radius.

The averaged plots and fitted power-law relationships are shown in figure 4.1 for one arbitrarily chosen simulation. The assumption of a power-law relationship appears to fit well with the data; however, it is the model's sensitivity to this assumption which is of interest to us.

In figure 4.2 it is obvious that the results from the simpler models, S1 and S2, have a much slower growth. This is as previous studies, including those by Passarelli and Srivastava [38] and the second by Sasyo and Matsuo [39], predicted. It is also physically intuitive: as the dispersion in velocities between the particles of larger sizes increased so did their probability of collision and consequently aggregation, therefore greater numbers of aggregations are likely to take place as are collisions between larger particles, which have a significant impact on the results. This second moment, proportional to the radar reflectivity, is used to compare the new modified Monte Carlo model with the simpler

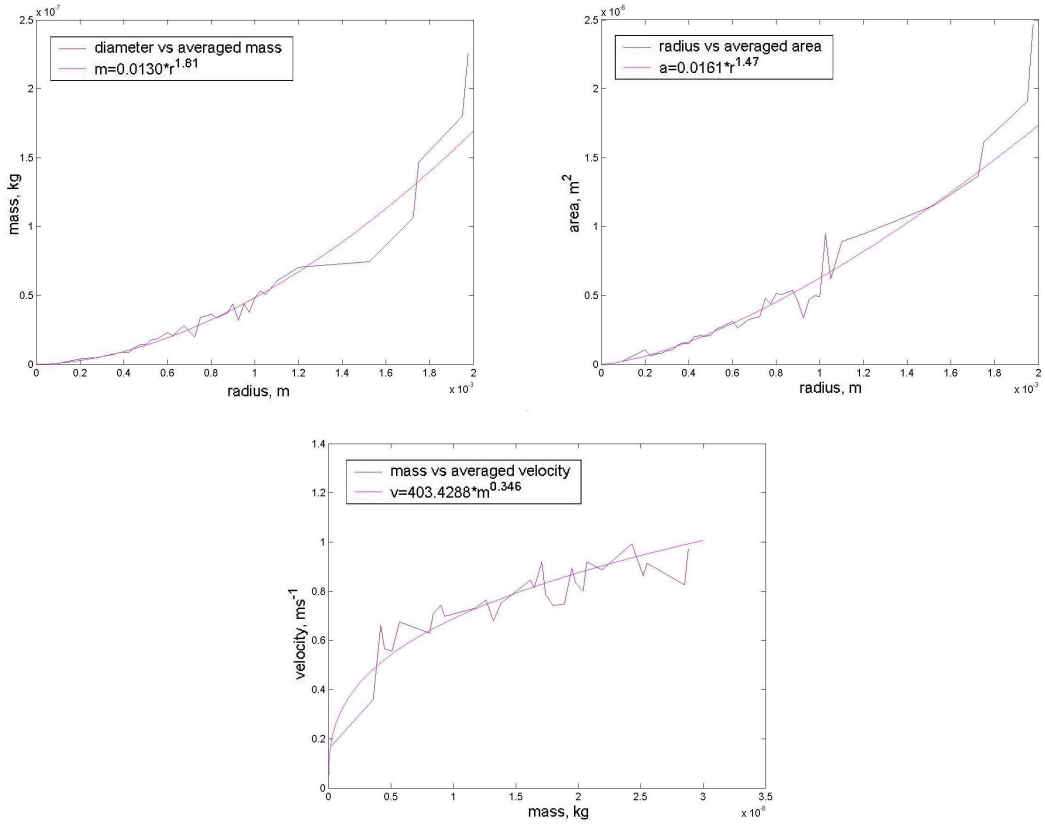

Figure 4.1: The plots and fitted power law relationships are shown for mean velocity against mass, mean area against radius and mean mass against radius.

versions instead of the averaged diameter because the simpler models by-pass the actual shapes of the particles and the diameter is effectively made a function of mass. This means that the diameter does not play a role in the growth.

4.2 Effect of velocity dispersion on Doppler radar measurements

Doppler radar can be used to measure properties of ice crystals in clouds. As discussed in section 3.5 these include the Doppler velocity, which is equivalent to the average speed at which the particles falls towards the radar, and the reflectivity, higher values of which correspond to the larger hydrometers seen lower in the cloud. However the Doppler spectrum measurements acquired from radars may hold the key for more detailed and extensive observational data. There is the potential to obtain estimates for parameters including the ice water content and average particle size. This would require

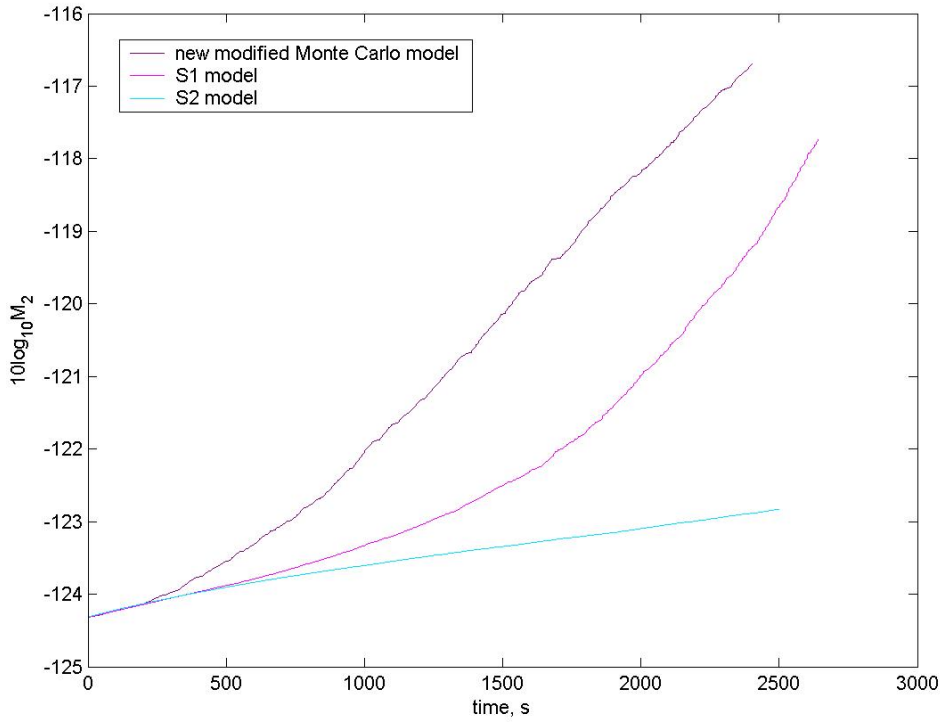

Figure 4.2: Plot of M2 vs time for the three models using variable values $n = 50000$, $t/2a = 0.1$, $t = 20 \times 10^{-6}$ $W = 10$ finishing at 2500 seconds

assumptions: that a relationship between the velocity and mass exists and that the size distribution follows a known function, probably exponential. We therefore must check whether making these assumptions in this situation is reasonable or if assuming the velocity can be calculated using a simple velocity-mass relationship produces an altered spectrum.

To test this, the summation of the mass squared, $\sum m^2$, will be studied as a function of the velocity. The Doppler spectrum, which is $\propto \sum_{bin} m^2$/bin width as a function of v, is produced using the assumed 1-to-1 velocity mass fit and is compared with the 'real' spectrum where all the variability of different snowflake shapes are taken account of. To produce a plot of this without the assumptions, a 'normal' output, the particles will be allocated to bins according to their velocity. The mass for each particle is then squared and added to the $\sum m^2$ that corresponds to its velocity-designated bin. The total $\sum m^2$ for each bin is then plotted against the velocity. To assume the relationship between velocity and mass a 'simplified' output is calculated. The particles are binned by mass, rather than velocity, and each particle's mass is squared and added to the $\sum m^2$ corresponding to the bin. Before the data collected for each bin is output by the

model the velocity is calculated assuming the velocity-mass relationship. This is done using the method for a velocity-mass relationship described for the S2 model in section 4.1.

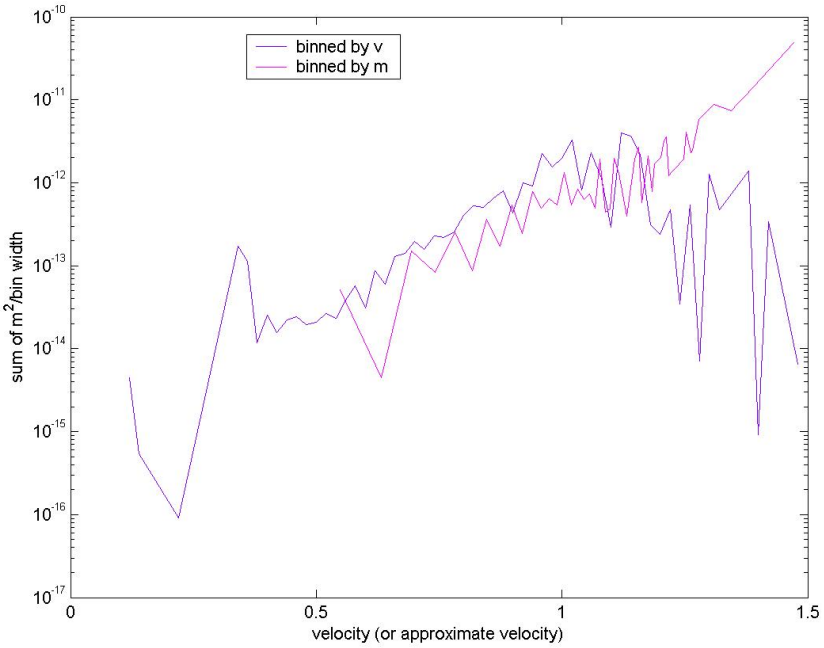

Figure 4.3: Plot of results of 'normal' and $v\,(m)$ fitted Doppler spectrum

Figure 4.3 shows that the Doppler spectrum produced with and without the underlying assumptions. The plots both exhibit noise which is to be expected as all the plots produced using a method that involved using bins have done so. The general form of the spectrum, without assuming a velocity-mass relationship, appears to be approximately parabolic in shape. When a velocity-mass relationship is assumed then the spectrum produced appears to match the 'normal' spectrum in the centre however as the velocity becomes large the $\sum m^2$ does not decrease as expected, but remains at a reasonably high level. This behaviour was common throughout all attempted parameter variations.

In general the assumptions that are needed to obtain estimates of ice crystal parameters appear to be reasonable; however the behaviour exhibited for larger velocities is unexpected. It is possible that this behaviour is an artifact of the method by which these results where produced within the model but this behaviour is an issue that merits further investigation.

Chapter 5

Conclusions

5.1 Summary

In this dissertation the effect of the variability in snowflake shape on aggregation was studied and found to be influential in some results but not all.

A literature review of previous studies on aggregation was used to build the picture produced so far. Particular attention was paid to studies which related to the fall speeds of ice particles as the fall speeds control the aggregation process through collisions produced by ice particles falling at different velocities. Calculations of the fall speed from Mitchell and Heymsfield [9] were used within a new modified Monte Carlo model to produce a model that accounted for the effects of individual snowflakes shapes. Observational studies and results were also reviewed, to be used later for comparison, as were other models.

The results presented in this dissertation are produced using a modified version of the Westbrook et al Monte Carlo model described in section 2.3.3. The ice crystals used in the model are hexagonal plates, this is a compromise as although it has been argued by Jiusto and Weickmann in [36] that large snowflakes would be expected to predominately be aggregates of dendritic crystals, this would be very computationally expensive to model, especially accounting for the individual geometry of each aggregate. The results shown here and in Westbrook et al [2] suggest that many of the results are insensitive to the choice of initial crystal. The model also uses an improved representation of the aggregate fall speed using equation (2.19) so the particles now span a range of flow regimes rather than all existing in the same one, and their projected area is explicitly calculated.

The effects of these modifications on the new Monte Carlo model were tested, as

was the model's sensitivity to parameter changes. This was first done by observing the the mass-diameter relationship. Previous observations and studies, including Locatelli and Hobbs [13] and Heymsfield et al [11] have suggested that a realistic mass-diameter relationship would be of the form $m \propto D^{d_f}$ where $d_f \approx 2$. As shown in section 3.1 with figures 3.2 to 3.5 this appears to be true within the model irrespective of the parameters used. Therefore the model has managed to capture an important relationship found in observational studies.

The plots produced of the size distribution, seen in figure 3.12, could be exponential in nature as suggested by the generally accepted relationship $n(D) = N_0 \exp(-\lambda D)$. However the noise in the plots is too great for any definitive conclusions to be made on this. Integration from the largest particle size downwards allowed the exponential shape to be confirmed as shown in section 3.4.2.

A large part of this dissertation has tested the results from the new modified Monte Carlo model against hypotheses and results from other studies. Particular focus has been paid to the hypotheses that concern the evolution of velocity and aggregation for larger particles.

The evolution of average diameter through time was also studied as one measure of the aggregation rate. Figure 3.11 is typical of the plots studied, with steady growth appearing to continue even as the size distribution gets broader. This contradicts the study by Mitchell and Heymsfield [9] where they hypothesised that as the size distribution broadened aggregation would cease to be the dominant growth mechanism. However as the model only simulates aggregation and a steady growth in the average diameter is still observed as it becomes large then the rate of aggregation is clearly not decreasing.

Mitchell and Heymsfield's hypothesis was based upon the assumption that the dispersion of fall speeds between large snowflakes of different sizes reduces to negligible amounts if their diameters are large enough. While the bin averaged velocity against diameter plots, as seen in figure 3.6, did seem to conform to this assumption, when a more detailed picture was investigated it appeared that the situation was more complex. Plots of fall speeds of individual aggregates against its diameter, as seen in figures 3.7 and 3.8, revealed the prospect that, within this model at least, for larger diameters the dispersion between fall speeds was not negligible and was produced by variability in snowflake shape. This was further investigated using measurements of the standard deviation, as it has no bias on the quantity of data points available for each diameter bin. The standard deviation of the velocity did decrease as the diameter of the particle became large. However, as displayed in figures 3.9 and 3.10 it in no way became a neg-

ligible amount. Around the diameter sizes that Mitchell and Heymsfield suggested the fall speed variability would become negligible the standard deviation remains at almost 20% of the average fall speed.

The relationship between the parameters N_0 and λ was also investigated, as this has been a focus of interest in many studies, including Lo and Passarelli [16] and Mitchell et al [18]. Several methods were attempted to estimate the evolution of the relationship. The first of these methods involved plotting the evolution of the size distribution and produced no real results due to problems with noise. The next method used moments of the size distribution and was successful in producing a recognisable relationship between N_0 and λ when the lower order moments were ignored. These results showed a relationship that was approximately a power-law which was as expected and in that appeared to recreate the 'stage 2' of N_0 and λ evolution as observed by [16] and predicted by the Snow Growth Model in [18]. However, the 'stage 3', to which most study is currently devoted to and Mitchell et al attributed to a significant reduction in the aggregation rate, at λ 10cm^{-1} could not be reached by this method. Using any variation in the moments within the calculation produced very different $N_0 - \lambda$ curves, indicating that the method was unreliable. The last method attempted was an estimation of the integration of the size distribution and a study of its evolution. This method not only reproduced the afore-mentioned 'stage 2' of a power law but continued this relationship past the marker of $\lambda \approx 10\text{cm}^{-1}$ set by Mitchell et al and Lo and Passarelli for the radical change in behaviour. As this modified Monte Carlo model concentrates solely on aggregation this suggests that aggregation does not slow significantly which relates well to the results produced by the model on the dispersion of fall speeds for larger diameters but conflicts with the hypothesis given in Mitchell et al's study.

This continuation of the N_0 and λ power law relationship for $\lambda < 10\text{cm}^{-1}$ also conflicts with airborne observations produced by Lo and Passarelli [16]. However, Lo and Passarelli did not attribute the change in the relationship, only suggesting that it may be due to the break-up of particles, whereas the model is restricted to aggregation, so another mechanism or feedback may be the cause of the observed 'stage 3' behaviour. Another possibility is that it could be caused by the instrumentation used to gather the data for [16]. In studies by Field et al [22] and Korolev and Isaac [21] the effects of ice crystals shattering on the houses of the probes or in the turbulence and wind shear created by them in similar experiments are studied. This would mean that the data would be lost from the observations about many large particles as they shatter but the smaller, shattered pieces of it could remain and be counted within the observations. These readings would not have been rejected or accounted for, and could cause the observations to

produce incorrect size distributions, especially further into the aggregation process or equivalently lower down the cloud where there is a greater concentration of large particles. The effect of particles shattering would be to produce incorrect size distributions with an increased number of small particles and a decreased number of large particles than is there in reality, leading to a steeper size distribution and a larger λ that the true value. This is in its effect analogous to the natural break-up mechanism suggested by Lo and Passarelli as the cause for the 'stage 3' behaviour in their observations. Korolev and Isaac used an observed correlation between the maximum observed particle size and the frequency of images containing multiple fragments of particles being observed in the data to substantiate the idea. Their results suggested that for aggregates, within the images taken for airborne observations, the percentage of images containing shattered particles could be as high as 10%. Field et al's study also suggests that the impact of the shattering particles on the results would be significant with the difference in concentrations in particle size distributions being changed by up to a factor of 4 for some studies. They also showed evidence that the broader the size distribution became, which corresponds to the lower values of λ, the greater the effect the shattering would have on the results. This could possibly explain the results seen in Lo and Passarelli's results for N_0 and λ as suggested very recently by Heymsfield et al in [34] however it is in no way certain.

The second moment of the particle mass distribution was used to produce comparisons with data on reflectivity, Z taken from the 8.6mm Doppler radar at the Chilbolton observatory in Hampshire. This parameter has been observed to grow approximately exponentially with time, as seen in section 3.5, so it appears as a linear relationship on a logarithmic scale, dBZ units, of the data from the model. The data from the model is output at $10 * \log_{10} M_2$ which is proportional to dBZ and is observed in figure 3.18 to also have an approximately exponential relationship with time in agreement with the radar data, see figure 3.19. This supports Westbrook et al's [35] hypothesis that this exponential relationship is a "signature" signature of the mechanism of aggregation.

Lastly the modified Monte Carlo model was compared with simplified versions using assumptions of power-law relationships that are prevalent in studies on ice crystal aggregation. The results showed that the simpler models grew at a significantly slower rate than the new modified Monte Carlo model. This suggests that the effect of the variability in snowflake shapes is influential and cannot be in general ignored, and suggests that fitted relationships as used to define many variables in many studies, are possibly not the best method of snowflake modelling.

The implications of the velocity dispersion on using radar measurements to obtain

more extensive observations on ice clouds was also investigated as this would involve the assumption of a calculable velocity-mass relationship. The results showed that for most velocities, and hence diameters, the effect on the Doppler spectrum was not too discernible. However, for the highest velocities there was an unexpected change with the $\sum m^2$ remaining large when to produce the observed parabolic shape it should reduce. This behaviour is intriguing and merits further investigation.

5.2 Possible further work

As results in this dissertation have shown the dispersion of velocity and its effects merit further investigation. As well as investigation into the wider issue of its effects the results have exposed several areas that also merit further study.

More sensitivity tests should possibly be carried out looking at the mass-diameter relationship and velocity dispersion amongst others.

With further availability of more powerful computational units bigger simulations could be run to improve the statistics on results like the size distribution.

The behaviour of the Doppler spectrum plot for large velocities is interesting and it would be interesting to see if it is an artifact of the method used in producing the plot.

Other mechanisms could be built into the model and this could be evaluated to see how this changes the results and how the mechanisms react to each other. In particular calculation of the efficiency of aggregation against deposition as a growth mechanism in various temperature and super-saturation regimes in order to process how these affect which mechanism is dominant.

Bibliography

[1] Westbrook, C. D., R. C. Ball, P. R. Field and A. J. Heymsfield: Universality in Snowflake Aggregation *Geophysical Research Letters*, **31**, 2004, L15104.

[2] Westbrook, C. D., R. C. Ball, P. R. Field and A. J. Heymsfield: Theory of growth by differential sedimentation, with application to snowflake formation Physical Review, **70**, 2004, 021403.

[3] Westbrook, C. D.: Universality in snowflake formation Phd thesis, 2004.

[4] Van Dongen, P. G. J. and M. H. Ernst: Dynamical scaling in the kinetics of clustering Phys. Rev. Lett., **54**, 1985, 1396-1399.

[5] Mitchell, D. L.: Use of Mass- and Area-Dimensional Power Laws for Determining Precipitation Particle Terminal Velocities *Journal of the Atmospheric Sciences*, **53**, 1996, 1710–1722.

[6] Abraham, F. F.: Functional dependence of drag coefficient of a sphere on Reynolds number *Phys. Fluids*, **13**, 1970, 2194–2195.

[7] Knight, N. C. and A. J. Heymsfield: Measurement and interpretation of hailstone density and terminal velocity *Journal of the Atmospheric Sciences*, **40**, 1983, 1510–1516.

[8] Heymsfield, A. J. and M. Kajikawa: An improved approach to calculating terminal velocities of plate-like crystals and graupel *Journal of the Atmospheric Sciences*, **44**, 1987, 1088–1099.

[9] Mitchell, D. L. and A. J. Heymsfield: Refinements in the Treatment of Ice Particle Terminal Velocities Highlighting Aggregates *Journal of the Atmospheric Sciences*, **62**, 2005, 1637–1644.

[10] Khvorostyanov, V. I. and J. A. Curry: Terminal velocities of droplets and crystals: Power laws with continuous parameters over size spectrum *Journal of the Atmospheric Sciences*, **59**, 2002, 1872–1884.

[11] Heymsfield, A. J., S. Lewis, A. Bansemer, J.Iaquinta, L. M. Miloshevich, M. Kajikawa, C. Twothy and M. R. Poellot: A general approach for deriving the properties of cirrus and stratiform ice cloud particles *Journal of the Atmospheric Sciences*, **59**, 2002, 3–29.

[12] Bohm, H. P.: A general equation for the terminal fall speed of solid hydrometers *Journal of the Atmospheric Sciences*, **46**, 1989, 2419–2427.

[13] Locatelli, J. D. and P. V. Hobbs: Fall Speeds and Masses of Solid Precipitation Particles *Journal of Geophysical Research*, **79**, 1974, 2185–2197.

[14] Magono, C. and C. V. Lee: Meteorological classification of natural snow crystals *Journal Fac. Sci. Hokkaido Univ.*, **Ser. 7.2**, 1966, 321–362.

[15] Zikmunda, J. and B. Vali: Fall patterns and fall velocities of rimed ice crystals *Journal of Atmospheric Sciences*, **29**, 1972, 1334–1347.

[16] Lo, K. K. and R. E. Passarelli: The growth of snow in winter storms: An airborne observational study *Journal of Atmospheric Sciences*, **39**, 1982, 697–706.

[17] Wilson, D. R., S. P. Ballard: A microphysically based precipitation scheme for the UK meteorological office unified model *Quarterly Journal of the Royal Meteorological Society*, **125**, 1999, 1607–1636.

[18] Mitchell, D. L., A. Huggins and V. Grubisic: A new snow growth model with application to radar precipitation estimates *Atmospheric Research*, **82**, 2006, 2–18.

[19] Passarelli Jr, R. E.: An approximate analytical model of the vapor deposition and aggregation growth of snowflakes *Journal of the Atmospheric Sciences*, **35**, 1978, 118–124.

[20] Barthazy, E. and R. Schefold: Fall velocity of snowflakes of different riming degree and crystal types *Atmospheric Research*, **82**, 2006, 391–398.

[21] Korolev, A. and Isaac, G. A.: Shattering during sampling by OAPs and HVPS. Part I: Snow Particles *Journal of atmospheric and oceanic technology*, **22**, 2005, 528–542.

[22] Field, P. R., A. J. Heymsfield and A. Bansemer: Shattering and particle interarrival times measured by optical array probed in ice clouds *Journal of Atmospheric and Oceanic Technology*, **23**, 2006, 1357–1371.

[23] Baran, A. J.: On the scattering and absorption properties of cirrus cloud *Journal of Quantitive Spectroscopy and Radiative Transfer*, **89**, 2004, 17–36.

[24] Heymsfield, A. J., G-J van Zadelhoff, D. P. Donovon, F. Fabry, R. J. Hogan and A. J. Illingworth: Refinements to ice particle mass dimensional and terminal velocity relationships for ice clouds. Parts I and II *Journal of the Atmospheric Sciences*, **64**, 2007, 1047–1067 and 1068–1088.

[25] `http://snowflakebentley.com`, Dedicated to Wilson "Snowflake" Bentley's life's work and images, (last checked on 04.08.2008).

[26] Field, P. R., and A. J. Heymsfield: Aggregation and scaling of ice crystal size distributions *Journal for Atmospheric Sciences*, **60**, 2003, 544–560.

[27] Intergovernmental Panel on Climate Change (IPCC): *Climate Change 2007: Synthesis Report*, Avaliable from `http://www.ipcc.ch`, 2007.

[28] A. J. Heymsfield and J. Iaquinta: Cirrus Crystal Terminal Velocities *Journal of Atmospheric Sciences*, **57**, , 916–938.

[29] Rogers, R. R. and M. K. Yau: *A short course in cloud physics*, Oxford: Pergamon, 1989.

[30] Mason, B. J.: *The physics of clouds*, Oxford University Press, 1971.

[31] Hosler, C. L., D. C. Jensen and L. Goldshlak: On the aggregation of ice crystals to form snow *Journal of Meteorology*, **14**, 1957, 415–420.

[32] Pruppacher and Klett: *Microphysics of clouds and precipitation*, Kluwer Academic publishers, 1997.

[33] Bentley, W. A., and W. J. Humphreys: *Snow crystals*, Dover, 1962.

[34] Heymsfield, A. J., P. Field and A. Bansemer: Exponential size distributions for snow, *Journal of Atmospheric Sciences*, Not yet published.

[35] Westbrook, C. D., R. J. Hogan, A. J. Illingworth and E. J. O'Connor: Theory and observations of ice particle evolution in cirrus using Doppler radar: Evidence for aggregation *Geophysical Research Letters*, **34**, 2007, LO2824.

[36] Jiustoa, J. E. and H. K. Weickmann: Types of Snowfall *Bulletin of American Meteorological Society*, **54**, 1973, 1148–1162.

[37] `http://www.met.rdg.ac.uk/radar/ufam/copernicus.html`, The University of Reading Meteorology department's radar group's page on the cloud radars at Chilbolton, (last checked on 14.08.2008).

[38] Passarelli R. E. Jr, and R. C. Srivastava: A new aspect of snowflake aggregation theory *Journal of Atmospheric science*, **36**, 1979, 484.

[39] Sasyo Y. and T. Matsuo: Effects of the variations of falling velocities of snowflakes on their aggregation *Journal Met. Soc. Japan*, **63**, 1985, 249.